SOUTHERN PLAINS
TRANSPORTATION CENTER

Rehabilitation of Deteriorated Timber Piles Using FRP Composites

FATMIR MENKULASI, P.E., PH.D.
HADI BAGHI, PH.D.
DAVID HALL, PH.D.
NAHID FARZANA, MSC.

SPTC15.1-43-F

Southern Plains Transportation Center
201 Stephenson Parkway, Suite 4200
The University of Oklahoma
Norman, Oklahoma 73019

TECHNICAL REPORT DOCUMENTATION PAGE

1. REPORT NO.	2. GOVERNMENT ACCESSION NO.	3. RECIPIENTS CATALOG NO.
SPTC15.1-43		

4. TITLE AND SUBTITLE	5. REPORT DATE
Rehabilitation of Deteriorated Timber Piles using FRP Composites	December 30, 2017
	6. PERFORMING ORGANIZATION CODE
7. AUTHOR(S)	8. PERFORMING ORGANIZATION REPORT
F. Menkulasi, H. Baghi. D. Hall, N. Farzana	
9. PERFORMING ORGANIZATION NAME AND ADDRESS	10. WORK UNIT NO.
College of Engineering Louisiana Tech University 600 Dan Reneau Dr., Ruston, LA 71272	11. CONTRACT OR GRANT NO.
12. SPONSORING AGENCY NAME AND ADDRESS	13. TYPE OF REPORT AND PERIOD COVERED
Southern Plains Transportation Center 201 Stephenson Pkwy, Suite 4200 The University of Oklahoma Norman, OK 73019	Final June 2016 – June 2017
	14. SPONSORING AGENCY CODE

15. SUPPLEMENTARY NOTES

University Transportation Center

16. ABSTRACT

Louisiana has a large inventory of timber bridges in service. The timber piles in these bridges are succumbing to the effects of biological degradation that initiates in the wet-dry zones. Replacing these deteriorated piles is a costly process and in-situ repair of the piles with fiber reinforced polymers (FRP) is an economic alternative that does not require shoring the superstructure and does not interfere with the daily operation of the bridge. An experimental program was conducted to evaluate the capacity of FRP strengthened deteriorated timber piles under concentric and eccentric loads with different deterioration configurations. A total of 42 monotonic tests were conducted; 21 on concentrically loaded piles and 21 on eccentrically loaded piles. Three commercially available repair techniques were investigated to evaluate the efficiency of the repair with respect to restoring the original capacity of the pile. All repaired techniques were able to restore and typically enhance the original capacity of the undamaged piles. All failure modes were observed in the wooden portion of the pile outside the repaired region. The capacity of the repaired piles may be based on the undamaged timber portion of the pile. A method is presented to predict the axial load versus axial deformation relationship of concentrically loaded repaired piles. Strain gage measurements indicate that the FRP shell is mobilized more when the annular space is smaller due to the lower axial stiffness of the repaired pile compared to cases that feature larger annular spaces. Relative displacements between the repaired and unrepaired portions of the pile suggest that the repaired piles behaved compositely throughout the tests. Also, no sign of slip was observed at the top or bottom of the repair.

17. KEY WORDS	18. DISTRIBUTION STATEMENT
Timber piles; deterioration; fiber reinforced polymer composites; grout; repair; testing	No restrictions. This publication is available at www.sptc.org and from the NTIS.

19. SECURITY CLASSIF. (OF THIS REPORT)	20. SECURITY CLASSIF. (OF THIS PAGE)	21. NO. OF PAGES	22. PRICE
Unclassified	Unclassified	57	

SI* (MODERN METRIC) CONVERSION FACTORS

APPROXIMATE CONVERSIONS TO SI UNITS

SYMBOL	WHEN YOU KNOW	MULTIPLY BY	TO FIND	SYMBOL
		LENGTH		
in	inches	25.4	millimeters	mm
ft	feet	0.305	meters	m
yd	yards	0.914	meters	m
mi	miles	1.61	kilometers	km
		AREA		
in^2	square inches	645.2	square millimeters	mm^2
ft^2	square feet	0.093	square meters	m^2
yd^2	square yard	0.836	square meters	m^2
ac	acres	0.405	hectares	ha
mi^2	square miles	2.59	square kilometers	km^2
		VOLUME		
fl	fluid ounces	29.57	milliliters	m
oz	gallons	3.785	liters	L
gal	cubic feet	0.028	cubic meters	L
ft^3	cubic yards	0.765	cubic	m^3
yd^3	meters NOTE: volumes greater than 1000 L shall be			m^3
		MASS		
oz	ounces	28.35	grams	g
lb	pounds	0.454	kilograms	kg
T	short tons (2000 lb)	0.907	megagrams (or "metric ton")	Mg (or "t")
		TEMPERATURE (exact degrees)		
^oF	Fahrenheit	5 (F-32)/9 Celsius or (F-32)/1.8		^oC
		ILLUMINATION		
fc	foot-candles	10.76	lux	lx
fl	foot-Lamberts	3.426	candela/m^2	cd/m^2
		FORCE and PRESSURE or STRESS		
lbf	poundforce	4.45	newtons	N
lbf/in^2	poundforce per square inch	6.89	kilopascals	kPa

APPROXIMATE CONVERSIONS FROM SI UNITS

SYMBOL	WHEN YOU KNOW	MULTIPLY BY	TO FIND	SYMBOL
		LENGTH		
mm	millimeters	0.039	inches	in
m	meters	3.28	feet	ft
m	meters	1.09	yards	yd
km	kilometers	0.621	miles	mi
		AREA		
mm^2	square millimeters	0.0016	square inches	in^2
m^2	square meters	10.764	square feet	ft^2
m^2	square meters	1.195	square yards	yd^2
ha	hectares	2.47	acres	ac
km^2	square kilometers	0.386	square miles	mi^2
		VOLUME		
mL	milliliters	0.034	fluid ounces	fl oz
L	liters	0.264	gallons	gal
m^3	cubic meters	35.314	cubic feet	ft^3
m^3	cubic meters	1.307	cubic yards	yd^3
		MASS		
g	grams	0.035	ounces	oz
kg	kilograms	2.202	pounds	lb
Mg (or "t")	megagrams (or "metric ton")	1.103	short tons (2000 lb)	T
		TEMPERATURE (exact degrees)		
^oC	Celsius	1.8C+32	Fahrenheit	^oF
		ILLUMINATION		
lx	lux	0.0929	foot-candles	fc
cd/m^2	candela/m^2	0.2919	foot-Lamberts	fl
		FORCE and PRESSURE or STRESS		
N	newtons	0.225	poundforce	lbf
kPa	kilopascals	0.145	poundforce per square h	lbf/in^2

*SI is the symbol for the International System of Units. Appropriate rounding should be made to comply with Section 4 of ASTM E380.
(Revised March 2003)

ACKNOWLEDGEMENTS

This study was sponsored by the Southern Plains Transportation Center (SPTC). The authors are thankful for the opportunity to work on this project. The authors would also like to thank Denso North America, Simpson Strong Tie, and Pilemedic staff for their assistance in repairing the piles. Additionally, the authors would like to thank Simpson Strong Tie and Pilemedic for donating their materials for the second phase of testing. The opinions expressed herein are those of the authors and do not necessarily reflect the views of the sponsor.

REHABILITATION OF DETERIORATED TIMBER PILES USING FRP COMPOSITES

Final Report

December 2017

Fatmir Menkulasi, P.E., Ph.D., Assistant Professor

Hadi Baghi, Ph.D., Post-Doctoral Research Associate

David Hall, Ph.D., Associate Professor

Nahid Farzana, MSc., Graduate Research Assistant

Southern Plains Transportation Center

201 Stephenson Pkwy, Suite 4200

The University of Oklahoma

Norman, OK 73019

TABLE OF CONTENTS

LIST OF FIGURES

LIST OF TABLES

EXECUTIVE SUMMARY

Louisiana has a large inventory of timber bridges in service. The timber piles in these bridges are succumbing to the effects of biological degradation that initiates in the wet-dry zones. Replacing these deteriorated piles is a costly process and in-situ repair of the piles with fiber reinforced polymers (FRP) is an economic alternative that does not require shoring the superstructure and does not interfere with the daily operation of the bridge. An experimental program was conducted to evaluate the capacity of FRP strengthened deteriorated timber piles under concentric and eccentric loads with different deterioration configurations.

A total of 42 tests were conducted on undamaged, damaged, and repaired timber piles to characterize their behavior under concentric and eccentric loads. The repaired piles featured a FRP jacket, an underwater epoxy or grout fill and in some cases carbon fiber reinforcement between the FRP jacket and the timber pile. The repair materials are commercially available and were provided by Denso North America, Simpson Strong Tie and Pilemedic.

The repaired piles exhibited concentric axial load capacities that were not only in excess of those measured for the damaged piles but also typically surpassed the axial capacity of the reference undamaged pile regardless of which repair technique was used. The concentric load capacity of the damaged piles was increased by 82% to 420% by repairing them with FRP composites. Additionally, the original concentric load capacity of the undamaged pile was typically enhanced as a result of the repair with the exception of one pile for which the concentric load capacity was slightly lower than that measured for the undamaged pile. Similarly, the eccentric load capacity of the damaged piles was increased by 230% to 575% by repairing them with FRP composites regardless of the repair technique. The original eccentric load capacity of the undamaged piles was typically enhanced as well with the exception of three piles for which the eccentric load capacity was slightly lower than that measured for the undamaged pile. In general, the capacity of the repaired piles may be based on the wooden portion of the pile outside of the repair region if one of the repair techniques investigated in this study is adopted. A method was presented to predict the axial load versus axial deformation relationship for concentrically loaded repaired piles and it was shown that it leads to reasonable results given the variability in the wood material.

Strain gage measurements indicated that the FRP shell is mobilized more when the annular void is smaller. For 1 in. annular voids the mobilization of the FRP shell in terms of strains was less than 60% of the ultimate strain and for 2 in. annular voids it was less than 16% of the ultimate strain. The lower mobilization of the FRP shell for larger annular voids is

attributed to the fact that a larger annular void results in an increased axial and flexural stiffness in the repaired portion of the pile, which leads to smaller strains.

Small relative displacements were recorded between the wooden portion of the pile and the repaired portion due to differences in axial and flexural stiffness between these two components. No slip was observed at the pile-fill interface and all failures modes featured a material failure in the wooden portion of the pile outside the repair.

All investigated repair techniques are efficient and can be used to restore the capacity of damaged timber piles.

INTRODUCTION

Louisiana has a large inventory of timber bridges in service. The timber piles in these bridges are succumbing to the effects of biological degradation that initiates in the wet-dry zones of piles. The extent of the wet-dry zones is influenced by weather extremes such as droughts, extreme summer temperatures and flash floods. In many cases the deterioration of timber piles in the wet-dry zones occurs due to the presence of wood destroying fungi, which flourish in the presence of oxygen, moisture, and favorable temperatures. Figure 1 illustrates the type of damage typically observed in the wet-dry zone of timber piles in marine environments. The ideal combination of moisture and oxygen in the wet-dry zone leads to an hourglass shaped damage, which reduces the strength and stiffness of the original pile, undermining its original structural capacity. For this reason, the timber piles in many structures were cut-off below the lowest expected elevation of ground water table. However, for timber bridges in marine environments, the elimination of the wet-dry zone is not an option. Preservative treatments have been used for protection, however, environmental issues have restricted the use of these preservatives. Creosote, one of the most common and effective preservatives, has been banned in marine environments [1]. Also, the use of Chromate Copper Arsenate has been restricted in residential areas by the federal government and some states have banned it for noncommercial applications entirely [1].

a) b)

Figure 1. a) Marine borer attack of an 120 year old greenheart pile (© IHS, reproduced with permission from BRE Digest 479 [2]), b) hourglass shaped timber pile damage (reproduced with permission from Simpson Strong Tie [3])

The use of timber piles extends beyond bridge structures. Many building structures, ports, and piers are founded on timber piles and suffer from settlement induced damage as a

result of the deterioration of timber piles. In other cases, higher load demands in existing ports and piers require an upgrade of the existing foundations to meet the new load demands. As a result, it is imperative to identify effective rehabilitation techniques that restore and enhance the original capacity of the timber piles. Replacing the deteriorated piles is a costly process that requires posting the superstructure while the repair is taking place. Alternatively, in-situ repair of the piles with fiber reinforced polymer (FRP) composites is a more economic option, which does not interfere with the daily function of the bridge. Figure 2 illustrates the repair of a deteriorated pile using FRP composites. The first step typically involves the installation of prefabricated FRP shells, which serve as stay-in-place forms for the filler material. The second step involves the placement of the filler materials, which can be either an underwater grout or epoxy depending on the extent of the decayed portion of the pile. Epoxy is typically employed for piles with moderate decay, and grout is used for the more severely deteriorated piles to fill the larger annular void between the FRP jackets and the pile.

The goal of the research presented in this report is to identify commercially available rehabilitation techniques that can be used for the in-situ repair of deteriorated timber piles and characterize the performance of the repaired piles under concentric and eccentric axial loads.

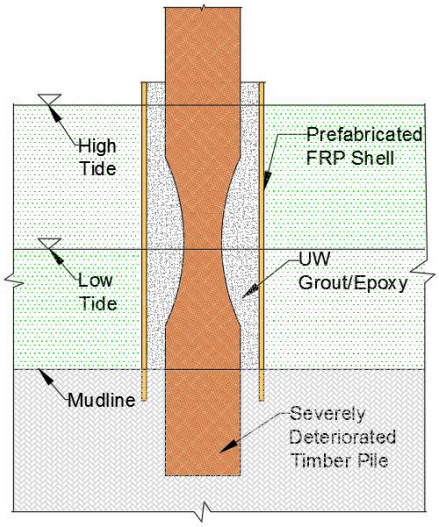

Figure 2. Typical repair of deteriorated timber piles using fiber reinforced polymer (FRP) composites

LITERATURE REVIEW

A state of the art literature review was conducted with an emphasis on the repair of the decayed timber piles using FRP composites. The following sections discuss damage characteristics in timber piles and various methods for restoring the original capacity of the piles.

Damage characterization

The characteristics of damage in timber piles vary. The focus of this report is the type of damage that leads to a reduced cross-section featuring an hourglass shape in the wet-dry zones of timber piles located in marine environments (Figure 1). This type of damage occurs due to the optimal combination of oxygen and moisture in the wet-dry zones, which leads to the deterioration of the pile as a result of wood destroying fungi and/or soft rot attack. Koppers [4] report that the critical decay zone is normally from 12 in. below ground surface to 12 in. above ground lines where there is typically the correct combination of moisture and oxygen. Similarly, Reynolds [2] states that untreated timber piles driven below the ground water table are virtually immune to biological degradation, however the section of the untreated pile above the groundwater table is vulnerable to decay. A similar characterization of the critical decay zone is reported by Tumialan et al. [5, 6] and Vatovec and Kelley [7, 8, 9] although it is noted that decay can also occur below the ground water table albeit at a lower rate.

Although areas outside of the wet-dry zone are typically not considered critical because there is a lack of either sufficient oxygen or moisture to initiate the deterioration of timber piles, they are subject to bacterial deterioration. Vatovec and Kelley [8] summarize potential deterioration mechanisms in timber piles as follows:

- Wood destroying fungi
- White and brown rot
- Soft rot
- Bacteria
- Marine borers
- Chemical hydrolysis

Bacterial attack is thought to occur always, at all sites, and in all conditions although the rate and degree of attack may vary depending on site specific conditions [5, 6, 7, 8, 9]. Marine borers also cause extensive damage to wood piles used to support piers, marinas, or other waterfront structures, and in many cases replacement of these piles has been the only alternative [10; 11]. In some other cases, the interior of the pile is damaged leading to a hollow cross-section [12, 13]. This type of damage was attributed to fungus infestation and as well as to the use of preservative treatment. Gopu and Avent [13] report that while it is well known that

preservative treatment adversely affects the mechanical properties of timber piles, the level of reduction in these properties in the undamaged portion of the piles was significantly higher than expected.

Protection of Timber Piles

One strategy for protection of wood piles from marine borer attack is encasing the new piles with plastic wrap or jacket [14; 15]. Most of the available methods are suitable only for protection and provide no structural restoration capabilities, and therefore, can only be used to protect new piles or piles with minimal damage and adequate structural properties [16]. More information on protection of timber piles including commercially available techniques is provided by Lopez-Anido et al. [16].

Restoring the Original Capacity of Damaged Piles

The service life of deteriorated timber piles can be prolonged in some cases by rehabilitating the piles. One common rehabilitation technique is to cut the entire portion of the pile above the decayed section and replace it with a new section (splicing). This method, while it restores the capacity of the damaged pile, it does not protect the pile from recurring damage. Another common method is that of removing only the decayed section and substituting it with a replacement stub (cutting and posting). Another repair strategy is replacing the damaged wood pile with a new concrete pile [17]. All of these methods require posting the superstructure while the repair is taking place.

Railway Track & Structures [18] explored a repair method that involved the injection of cementitious grout in decayed timber piles. The success of this method depends on the compatibility between the porosity of the decayed pile and the composition of the filler material.

Concrete jacketing is also a common repair technique. In this case, formwork (fabric or plastic) is installed around the decayed section of the pile. A reinforcing steel cage is placed between the pile and the formwork, and the annular void is filled with grout or concrete. Similarly, Chellis [19] proposes the use of a shotcrete jacket in lieu of the formed jacket. The disadvantage of these repair methods is the corrosion of reinforcing steel cage and spalling of the surrounding concrete.

A method for ground repair of wood poles has also been presented that involves screwing a metal sleeve around the base of the pole and filling the space between the sleeve and the pole with aggregates and resin [20; 21].

The use of FRP wraps and shells is another method to rehabilitate deteriorated piles.

Hagos [22] conducted an experimental study to evaluate the effectiveness of using Glass Fiber Reinforced Polymer (GFRP) systems and cementitious grout to restore heavily decayed timber piles to their original capacity. A similar method of repair was proposed by Emerson [23], which involves removing the decayed portion of the pile, filling the cavity with aggregate and epoxy to provide compression capacity, and finally wrapping the pile transversely with fiberglass to confine the repaired portion. In this method, the function of the GFRP wrap is only to provide confinement to the filler material and not act as a structural layer in the longitudinal direction. In addition, before the pile is wrapped with GFRP, some type of formwork is needed to hold the aggregate and resin in place. Hardcore Composites of New Castle, has developed a method, which is reported to protect as well as repair and restore timber piles. This system uses E-glass/vinyl ester composite shells fabricated by the vacuum-assisted resin transfer molding (VART) process. The shells are manufactured in two halves joined by using H connectors [16]. Fyfe Co. LLC, also known as the Fiberwrap Company, offers a method that uses a fabric reinforcement that is wrapped around the pile and then impregnated underwater with an epoxy resin providing a barrier against marine borers. Impregnation of the fabric reinforcement underwater is difficult to execute and monitor [16]. Lopez-Anido et al. [16] investigated a repair method, which utilizes FRP composite shells that encapsulate the deteriorated portion of the pile.

Some of the available protection and restoration methods have limited applicability in most cases. Concrete encasement can develop problems with spalling and fiber-reinforced composite jackets installed in halves have bonded longitudinal joints, that may limit the ability of the pile encasement to deliver circumferential confinement [16]. Additionally, application of wet fabric reinforcement underwater can be difficult, and proper curing of the resin may not be achieved [16].

To address the shortcoming of the wet layup method Pilemedic/QuakeWrap [24, 25] developed superlaminate™ shells that are prefabricated with the purpose of accelerating construction in the job site. In this repair technique the shells are wrapped around the pile and secured at the desired position creating an annular void with the decayed pile. Then a filler material is used to complete the repair. The superlaminate™ shells have the ability to deliver circumferential confinement. Similarly, Denso North America Inc. [26] offers a system called SeaShield™ Series 400 for the protection and strengthening of timber piles. The system consists of fiberglass forms, a carbon fiber grid that replaces the reinforcing steel mesh in traditional repair techniques, and a filler

material. Simpson Strong-Tie [3] offers a system called FX-70 for structural repair and protection purposes. The system consists of a high strength fiberglass interlocking jacket that features a tongue and groove vertical seam. The tongue-and-groove seamed jacket provides a corrosion-resistant shell to the repair site, ranges from 1/8 in. to ¼ in. thickness, and is UV-resistant. The filler materials is either FX-70-6PM Multi Purpose Marine Epoxy Grout or FX-225 Non-Metallic Underwater Grout.

From the repair systems described above the ones employed by Pilemedic/QuakeWrap Inc. [24, 25], Denso North America Inc. [26], and Simpson Strong-Tie [3] were selected for investigation. The rationale for this selection is related to the experimental evidence associated with these systems, commercial availability and relative ease of installation. All three repair systems can be implemented without the need to shore the superstructure and the composite FRP shells and have three functions: 1) they serve as stay-in-place formwork for the filler material, 2) they confine the filler material and hence increase its performance in compression, and 3) they provide marine borer protection.

CAPACITY OF FRP STRENGTHENED DETERIORATED TIMBER PILES

An experimental program was conducted to characterize the behavior of damaged piles rehabilitated with FRP composites under concentric and eccentric loads. A total of 42 tests were conducted, 21 of which featured concentrically loaded piles and the remaining 21 featured eccentrically loaded piles. While pile damage varies widely, an hourglass shaped reduction of the cross-sectional area was implemented to simulate observed damaged conditions in the wet-dry zone (Figure 1), which include a reduction in strength and stiffness [2]. The extent of damage in terms of depth and length was controlled to evaluate the efficiency of the repair techniques and to be able to draw generalized conclusions. All piles with the exception of the undamaged pile were taper cut into an hourglass shape resulting in five different deterioration zones. Figure 2 illustrates the configuration of the induced damage and features two damage depths and four damage lengths. The piles that featured a 1 in. damage depth represent moderate decay and those that feature a 2 in. damage depth represent severe decay. Damage lengths varied from 12 in. to 18 in. The nominal diameter of all piles is 8 in. and the material is Yellow Southern Pine. The actual diameter of each pile was measured and recorded. All piles were acquired from the same jungle and they were all treated with Chromate Copper Arsenate (CCA). Figure 4 illustrates the undamaged piles, the setup that was used to induce marine damage, and the intentionally damaged piles. A table saw was used to induce the damaged described in Figure 3. The depth of cut was adjusted such that it matched the desired depth at a

given location in the damaged region. Two adjacent blades were used to induce damage incrementally as shown in Figure 4.

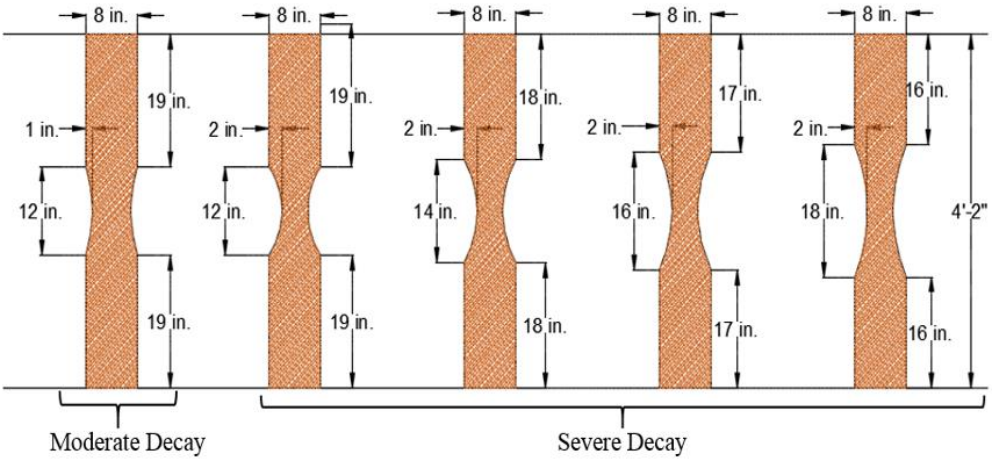

Figure 3. Configuration of induced damage

Figure 4. a) Undamaged piles, b) setup for inducing marine damage, c) damaged single pile, d) damaged group of piles

Table 1 illustrates the configuration of the tested piles in terms of damage length and depth. Two tests were conducted on undamaged reference piles (Test 1 and 22), ten tests were conducted on damaged unrepaired piles (Tests 2 through 6 and 23 through 27), and thirty tests

were conducted on damaged and repaired piles (Tests 7 through 21 and 28 through 42). The designation for each tested pile follows a one letter and two number format. The unrepaired piles were assigned the designation *R* (reference). The repaired piles were assigned a letter to represent the manufacturer of the repair products, *D* for Denso North America, *P* for Pilemedic, and *S* for Simpson Strong Tie. The first number represents the damage depth and the second number represents the damage length (both in inches).

Table 1: Configuration of tested timber piles

Test No.		Specimen ID	Damaged Length (in.)	Damaged Depth (in.)	Moisture Content (%)			
					Concentrically Loaded		Eccentrically Loaded	
Concentric	Eccentric				Before	After	Before	After
1	22	R-0-0	0	0	10	30	9	34
2	23	R-1-12	12	1	15	36	14	31
3	24	R-2-12	12	2	10	35	11	33
4	25	R-2-14	14	2	10	37	10	36
5	26	R-2-16	16	2	10	40	10	32
6	27	R-2-18	18	2	10	38	9	34
7	28	D-1-12	12	1	9	37	10	35
8	29	D-2-12	12	2	11	33	12	26
9	30	D-2-14	14	2	10	36	10	30
10	31	D-2-16	16	2	10	33	10	37
11	32	D-2-18	18	2	9	33	8	28
12	33	P-1-12	12	1	11	31	12	36
13	34	P-2-12	12	2	10	33	11	34
14	35	P-2-14	14	2	10	34	11	35
15	36	P-2-16	16	2	9	34	10	31
16	37	P-2-18	18	2	11	35	9	29
17	38	S-1-12	12	1	10	33	13	40
18	39	S-2-12	12	2	10	34	10	30
19	40	S-2-14	14	2	10	31	12	36
20	41	S-2-16	16	2	9	37	12	34
21	42	S-2-18	18	2	10	35	13	40
				Average	**10**	**35**	11	33
				COV (%)	**12**	**7**	14	11

All piles were fully saturated by immersing them in a water container. Table 1 illustrates the moisture content before and after saturation. After the initial moisture content of the piles was recorded, all piles were immersed in a water container and the moisture content was measured every three days using a moisture meter (Figure 5a). When moisture content readings reached the point where there was no appreciable increase between subsequent readings the piles were taken out of the water container and were prepared for repair. The amount of time that it took for the piles to be fully saturated was approximately 30 days. Figure 5b shows the moisture content as a function of time for 26 out of the 42 tested piles. After the piles were repaired they were immersed in the water container again for 30 days to allow the infill grout and epoxy to gain their design strength. The moisture content was measured only

after 30 days when the repaired piles were taken out of the water container and were prepared for testing. No intermediate moisture readings were taken between the time the piles were repaired and the time that they were tested due to the weight of the piles (approximately 300 lbs). However the moisture readings taken before the piles were tested are similar with those taken prior to the repair, which suggests that the piles were fully saturated during that time. The reference undamaged and damaged unrepaired piles were left in the water container until the day they were tested.

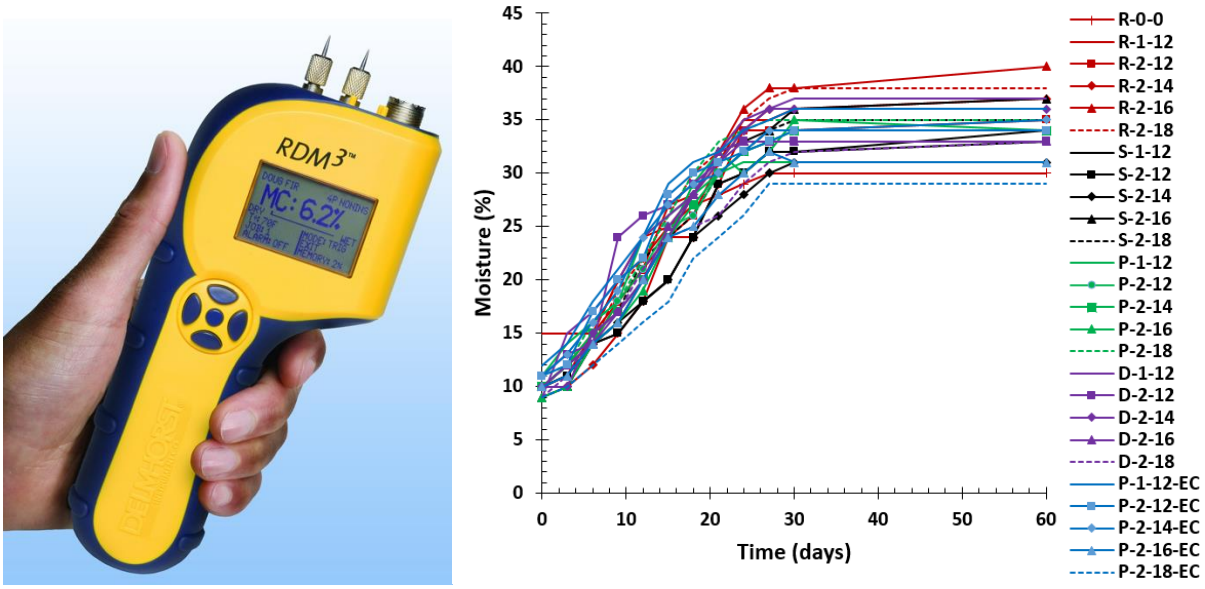

a) b)

Figure 5. a) Delmhorst Moisture Meter used to measure moisture content, b) moisture content versus time (source for (a):http://www.bestharveststore.com/Delmhorst-RDM3-Wood-Moisture-Meter-Plus-with-21E-Contact-Pins-and-Case-p229.html)

The average moisture content before the piles were immersed in water was 10% and 11% for concentrically loaded and eccentrically loaded piles, respectively, and the average coefficient of variation for each case was 12% and 14%, respectively. The average moisture content of the piles after they were immersed in water was 35% and 33% for concentrically loaded and eccentrically loaded piles, respectively, and the average coefficient of variation for each case was 7% and 11%, respectively. The coefficient of variation in the fully saturated piles was less than that calculated based on initial moisture content.

Figure 6 illustrates the repair techniques for piles with moderate and severe decay namely Repair Detail x1 and x2. The letter indicates the manufacturer of the repair products. In general all repair details featured a prefabricated FRP shell and underwater grout or epoxy to fill

the annular void. For severely decayed piles, Repair detail D2 featured the addition of a carbon fiber grid in the annual space prior to the placement of grout or epoxy. Repair detail S2 features a multi-purpose marine epoxy grout for the bottom 6 in. and the top 4 in. of the repaired region. The rest of the annular space is filled with non-metallic underwater grout. The prefabricated FRP jackets in details D1 and D2 feature a tongue and groove closure reinforced with stainless steel staggered rivets or screws at 6 in. on center maximum (Figure 7a). Similarly, the prefabricated FRP jackets in details S1 and S2 are 1/8 in. thick, round translucent jackets with a tongue and groove joint (Figure 7b). Self-tapping stainless steel screws are used along the joint seam to reinforce it. An 8 in. minimum overlap is employed between the two bidirectional jacket layers used in details P1 and P2 to provide closure (Figure 7c). The extent of the undamaged portion that is covered by the repair material is 8 in. above and below the decayed length for all repair details. The total length of piles is 50 in.

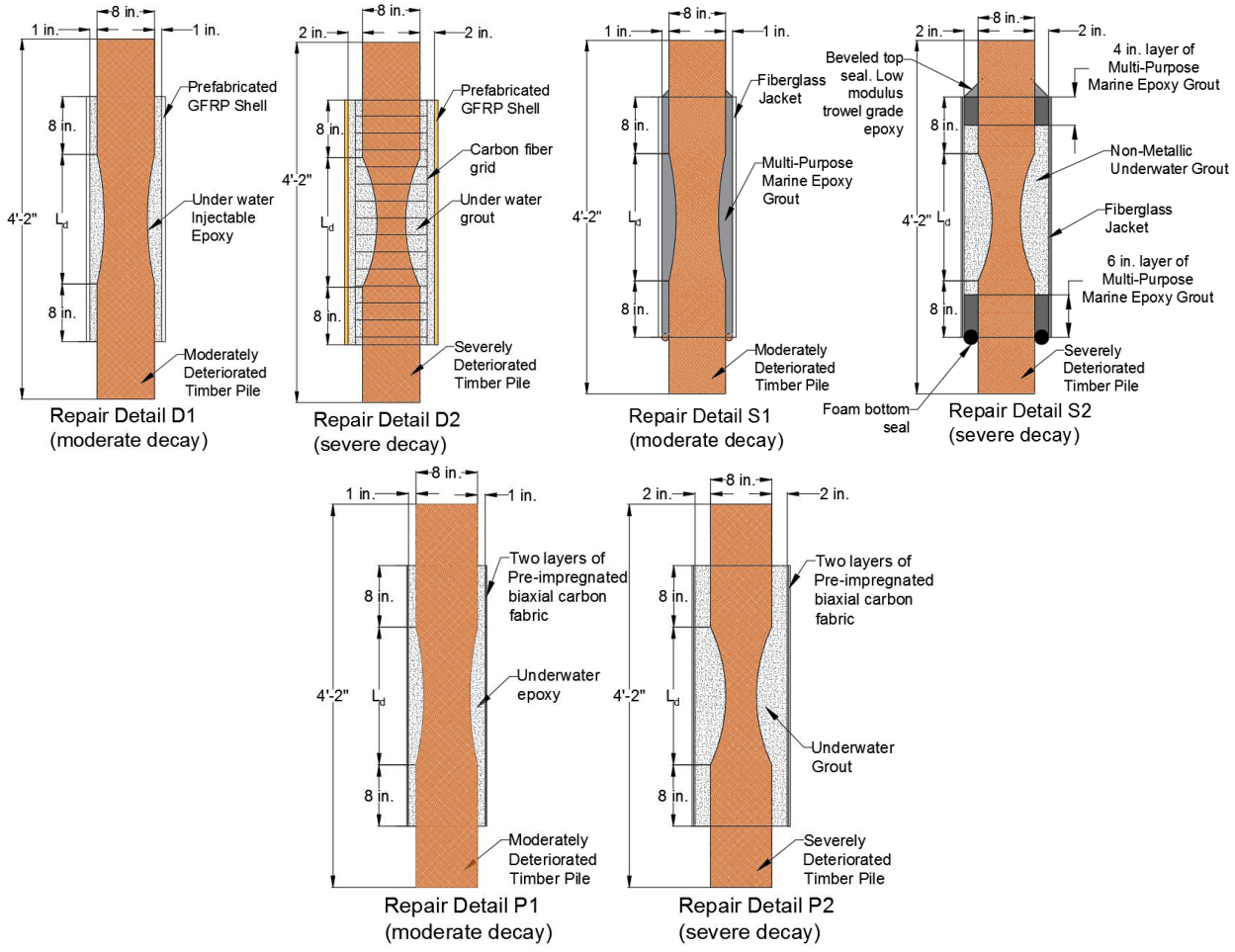

Figure 6. Repair details

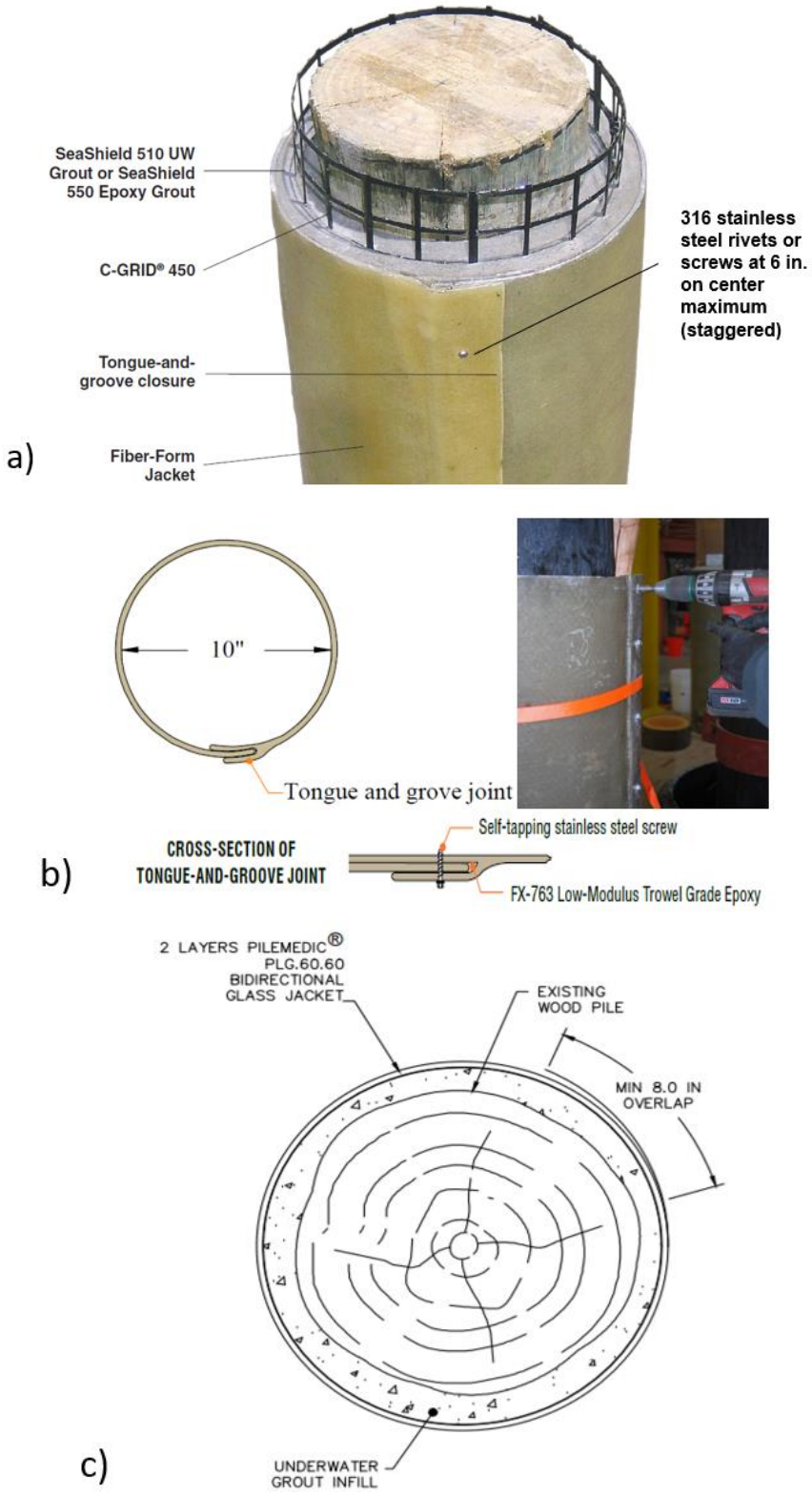

Figure 7. FRP jacket joint details, a) reproduced with permission from Denso North America, b) reproduced with permission of Simpson Strong Tie, c) reproduced with permission of Pilemedic

All repairs were executed by the personnel of the manufacturer of the repair products. Figure 8 shows the repair of the damaged piles with Denso North America products. All damaged piles were positioned vertically using cross shaped steel stands, which were bolted to the bottom of the piles. Plywood sheets were used at the bottom to serve as pour stops for the infill grout or epoxy. The carbon fiber grid was positioned in the desired location within the annular void. The prefabricated FRP jackets with the tongue and groove joint were installed by opening the joint enough to allow the insertion of the pile. Ratchet straps were used to secure the FRP jacket in the desired position. Then the annular void was filled with under grout water or epoxy depending on the extent of the induced damage. Finally, the ratchet straps and plywood pour stops were removed. This repair technique relies on the prefabrication of FRP jackets to match the diameter of timber piles and size of the desired annular void.

Figure 9 shows the repair of the damaged timber piles with Simpson Strong Tie products. The damaged piles were positioned vertically using the steel cross strands described earlier and the prefabricated FRP jackets were installed by opening the tongue and groove joint to receive the pile. The prefabricated FRP shell featured spacers on the inside to create the desired annual space. A foam seal was installed at the bottom to serve as a pour stop for the infill grout or epoxy. Nylon ratchets were used to additionally secure the FRP jacket in the desired position. For the piles that featured a 1 in. annular void, a multi-purpose marine epoxy grout was used as the fill material for the entire length of the repair. Whereas for the piles that featured a 2 in annular void, the multipurpose marine epoxy grout was used only for the bottom 6 in. and the top 4 in. of the repair. The rest of the annular space was filled with non-metallic grout. Finally, a low modulus trowel grade epoxy was used to bevel the top of the repair as shown in Figure 6 and Figure 9. This method also relies on the prefabrication of the FRP jackets to match the size of the decayed pile and the desired annular void.

Figure 10 shows the repair of the damaged timber piles with Pilemedic products. The damaged piles were secured vertically on the steel cross stands and spacers were installed above and below the damaged region to create the desired annular space. Plastic pour stops were installed at the bottom prior to the installation of the FRP laminates. The FRP laminates in this case came in flat sheets and were custom cut to match the diameter of the pile and the desired annular space. Two layers of bidirectional FRP laminates were wrapped around the damaged piles to create an 8 in. minimum overlap. After the spacers were installed, a coat of underwater epoxy was applied to the outside of the first FRP layer and the laminate was wound around the damaged pile to create an 8 in. minimum overlap (Figure 7c). Similarly, a coat of underwater epoxy was applied to the inside of the second FRP layer and the laminate was

wrapped around the first layer to create an 8 in. minimum overlap. Zip ties were used to additionally secure the laminates in the desired position and tie the plastic pour stops to the FRP laminates to seal any voids. Finally, the annular void was filled with either underwater epoxy or grout.

Figure 8. Repair of damaged timber piles – Densona

Figure 9. Repair of damaged timber piles – Simpson

Figure 10. Repair of damaged timber piles – Pilemedic

Axial Load Tests

A total of 21 tests were conducted on axially loaded piles. As shown in Table 1, one test was conducted on an undamaged pile, five tests were conducted on damaged unrepaired piles featuring various damage configurations, and 15 tests (five for each repair technique) were conducted on damaged and repaired piles using the repair methods illustrated in Figure 6. The damage configuration in the damaged and repaired piles matched the configuration of the damaged unrepaired piles so that the efficiency of the repair techniques could be evaluated. The goal was to compare the axial load capacities of damaged and repaired piles with those obtained for damaged and unrepaired piles and the undamaged pile. The test on the undamaged pile was conducted to establish a baseline for undamaged capacity as well as to characterize the behavior of wood material in terms of stress and strain. The tests on damaged unrepaired piles were conducted to quantify the reduction in axial load capacity caused by the induced damage.

Figure 11 illustrates the test setup for the concentrically loaded piles. A self-contained loading frame with a 400 kip capacity was used to test all piles. The actuator, which is part of the loading frame, reports axial load and vertical displacement. A total of three uniaxial electrical resistance strain gages were installed in the upper half of the pile to measure the vertical strain in the FRP shell. These strain gages are denoted V1, V2, and V3 (Figure 11). Additionally, three uniaxial electrical resistance strain gages were installed in the upper half to measure circumferential strain in the FRP shell. These strain gages are denoted H1, H2, and H3. The electrical resistance strain gages were installed to measure the mobilization of the FRP shell in resisting the applied loads. Vertical strain gages measure mobilization in terms of axial load resistance and composite action and the horizontally oriented strain gages measure the ability of the FRP shell to provide circumferential confinement. Two linear variable differential transducers (LVDTs) are used at the top and bottom of the pile to measure the difference between axial deformation in the wooden portion of the pile and the deformation at the beginning of the composite section. Some relative axial deformation is expected because of the difference in the axial stiffness between the wooden portion of the pile and the composite cross section.

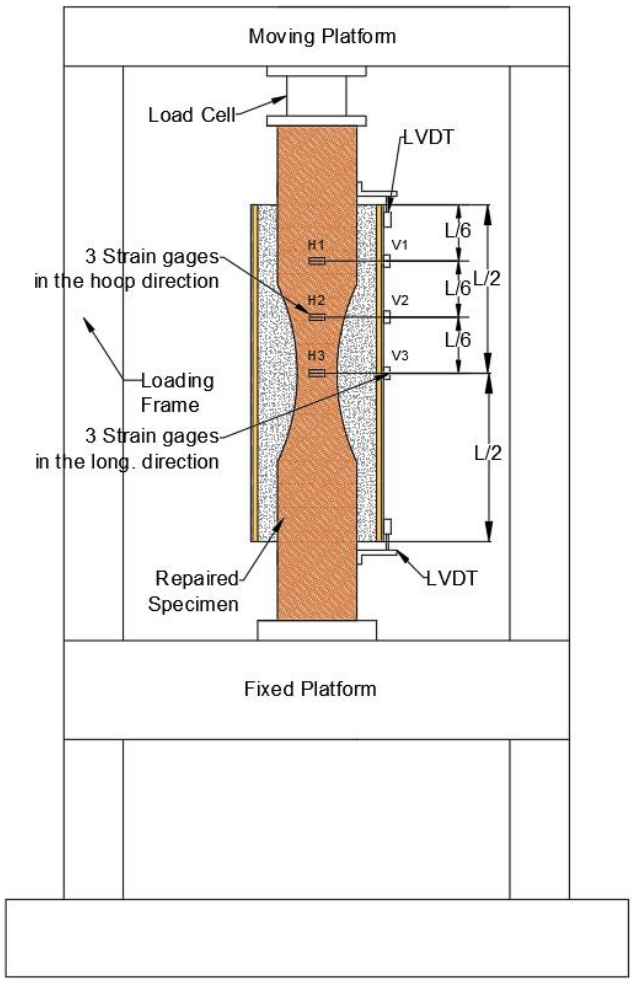

Figure 11. Test setup for concentrically loaded piles

Results of Axial Load Tests

Table 2 provides a summary of the maximum loads measured for all reference piles. The maximum load was divided by the net cross-sectional area to calculate the failure stress in the reference piles. The average failure stress was 2.5 ksi and the coefficient of variation was 15.2%. The differences in the peak stress are attributed to the variability of the wood material despite the fact that all samples were obtained from the same jungle. This variability stems from the presence of knots, orientation of grains, etc. All failure modes featured a material failure due to the short length of the piles. Figure 12 illustrates the failure mode in the undamaged pile and the damaged unrepaired piles. In both cases the failure occurred at mid-height of the pile. For the damaged unrepaired pile this was expected because the smallest cross section of the pile was at mid-height. For the undamaged pile the failure was expected to occur in the weakest cross section.

Table 2**:** Maximum load and stress in reference piles

Specimen No.	Max. load (kips)	Max. Stress (ksi)
R-0-0	135	2.5
R-1-12	74	2.6
R-2-12	31	2.2
R-2-14	50	3.1
R-2-16	31	2.1
R-2-18	41	2.7
	Average	**2.5**
	COV (%)	**15.2**

Figure 12: Testing of undamaged and damaged-unrepaired timber piles loaded concentrically

Table 3 provides a summary of the peak loads for all tested piles. The peak loads for the repaired piles were compared with the peak load of the undamaged pile as well as the peak load for the damaged pile that featured the same damage configuration. The peak load for the undamaged pile is 135 kips. The peak loads for the repaired piles vary from 125 kips to 181 kips. The ratios between the peak loads of repaired piles and damaged unrepaired piles varied from 1.98 to 4.83, which means that the repair can increase the axial capacity of the damaged pile from 98% to 383%. The ratios between the peak loads of repaired piles and undamaged pile varied from 0.93 to 1.22, which means that the repair not only restores the original axial capacity of the pile but also typically enhances it. In all repaired piles the failure took place in the portion outside the repair (Figure 13). There was only one repaired pile, which exhibited a lower axial capacity than the undamaged reference pile. The ratio between the repaired capacity and undamaged capacity in this case was 0.93. This small difference is attributed to the variability of the wood material given that all failures occurred in the wooden region of the pile outside of the repaired portion.

Table 3**:** Failure loads of all concentrically loaded specimens

Specimen No.	Length of damage (in.)	Depth of damage (in.)	Failure Load (kips)	Ratio = Repaired/Baseline	
				Ratio 1 = Repaired/Undamaged	Ratio 2 = Repaired/Damaged
R-0-0	0	0	135	NA	NA
R-1-12	12	1	74	NA	NA
R-2-12	12	2	31	NA	NA
R-2-14	14	2	50	NA	NA
R-2-16	16	2	31	NA	NA
R-2-18	18	2	41	NA	NA
D-1-12	12	1	147	1.10	1.98
D-2-12	12	2	151	1.13	4.83
D-2-14	14	2	162	1.20	3.21
D-2-16	16	2	138	1.03	4.46
D-2-18	18	2	164	1.22	3.99
P-1-12	12	1	135	1.00	1.82
P-2-12	12	2	163	1.21	5.20
P-2-14	14	2	181	1.35	3.61
P-2-16	16	2	144	1.07	4.62
P-2-18	18	2	144	1.07	3.52
S-1-12	12	1	162	1.20	2.18
S-2-12	12	2	136	1.01	4.32
S-2-14	14	2	168	1.25	3.34
S-2-16	16	2	125	0.93	4.03
S-2-18	18	2	151	1.12	3.67
			Average	**1.13**	**3.65**
			COV (%)	**10**	**20**

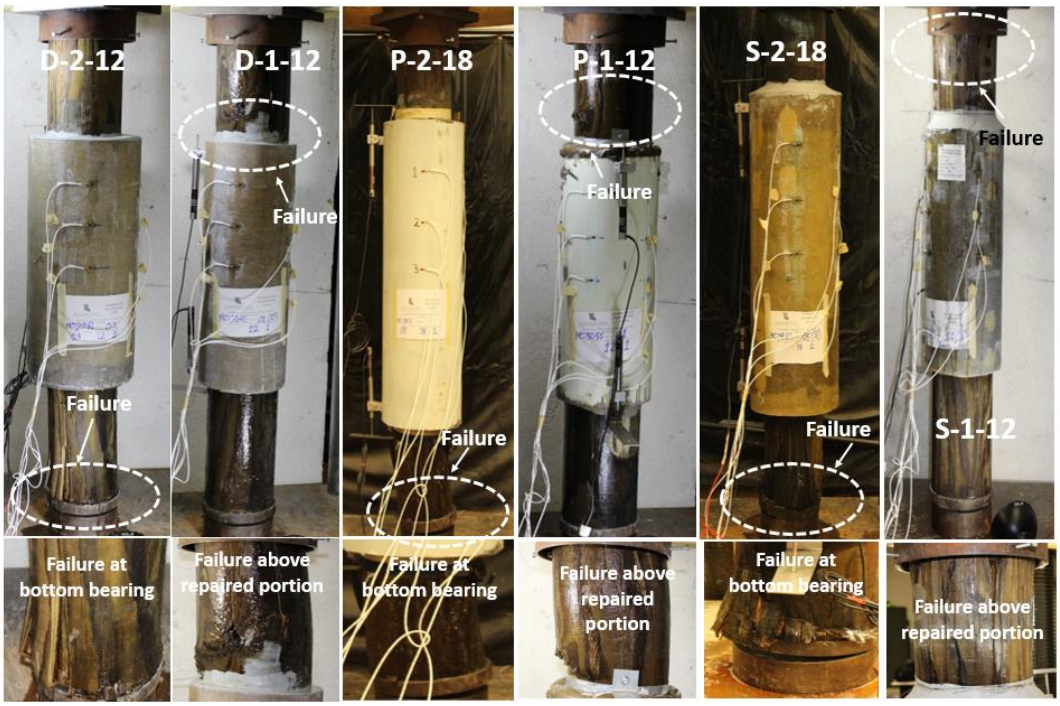

Figure 13: Testing of concentrically loaded repaired timber piles and illustration of failure mode

Figure 14 illustrates the measured load versus vertical displacement diagrams for all tested piles. This figure once again illustrates that the repair not only restores the original

capacity of the timber pile but it typically also enhances it. The measured load versus axial deformation relationship was compared with predicted values by assuming full composite behaviour between the timber pile and the repair materials. The predicted load versus axial deformation relationship was obtained using the principles of engineering mechanics and constitutive relationships for each material. Figure 15 shows the stress versus strain diagrams for each material. The stress-strain curve for timber was obtained by diving the applied load by the cross-sectional area of the undamaged pile to obtain stress and by dividing the measured displacement by the total length of the pile to obtain strain. The stress-strain curve for timber is almost linear and it exhibits a slightly softening behaviour near the peak stress. The stress-strain curve for the FRP shells was created using uniaxial tensile data provided by each manufacturer and by assuming that the uniaxial behaviour of the FRP shell in tension and compression was identical. The strength and stiffness of the FRP shells provided by Densona and Simpson are similar. The FRP shells provided by Pilemedic are stiffer and stronger. The utilization of these FRP shells in terms of structural capacity is discussed later in this report. The stress-strain curves for grout and epoxy were obtained using the concrete material constitutive model provided in Eurocode 2 [27] and are illustrated in Figure 15. The adopted stress-strain relationship is described in Eq. 1 and is illustrated in Figure 16. Table 4 provides the necessary values to construct the stress-strain curve. The only required input for this model is the design compressive strength for grout and epoxy, which was obtained from the manufacturer's literature. The stress-strain curves for the grout provided by Pilemedic and Densona are very similar and are stronger than that provided by Simpson. The stress-strain curves for the epoxy provided by Simpson and Densona are very similar and are stronger than that provided by Pilemedic.

$$\frac{\sigma_c}{f_{cm}} = -\frac{kn-n^2}{1+(k-2)n} \text{ for } |\varepsilon_c| < |\varepsilon_{c,lim}| \quad (1)$$

where:

$n = \varepsilon_c/\varepsilon_{c1}$

ε_{c1} = strain at maximum compressive stress (Table 4)

$k = \frac{E_{ci}}{E_{c1}}$ = plasticity number according to Table 4

E_{c1} = secant modulus from the origin to the peak compressive stress (Table 4)

$E_{ci} = 22(\frac{f_{cm}}{10})^{0.3}$ (f_{cm} in MPa)

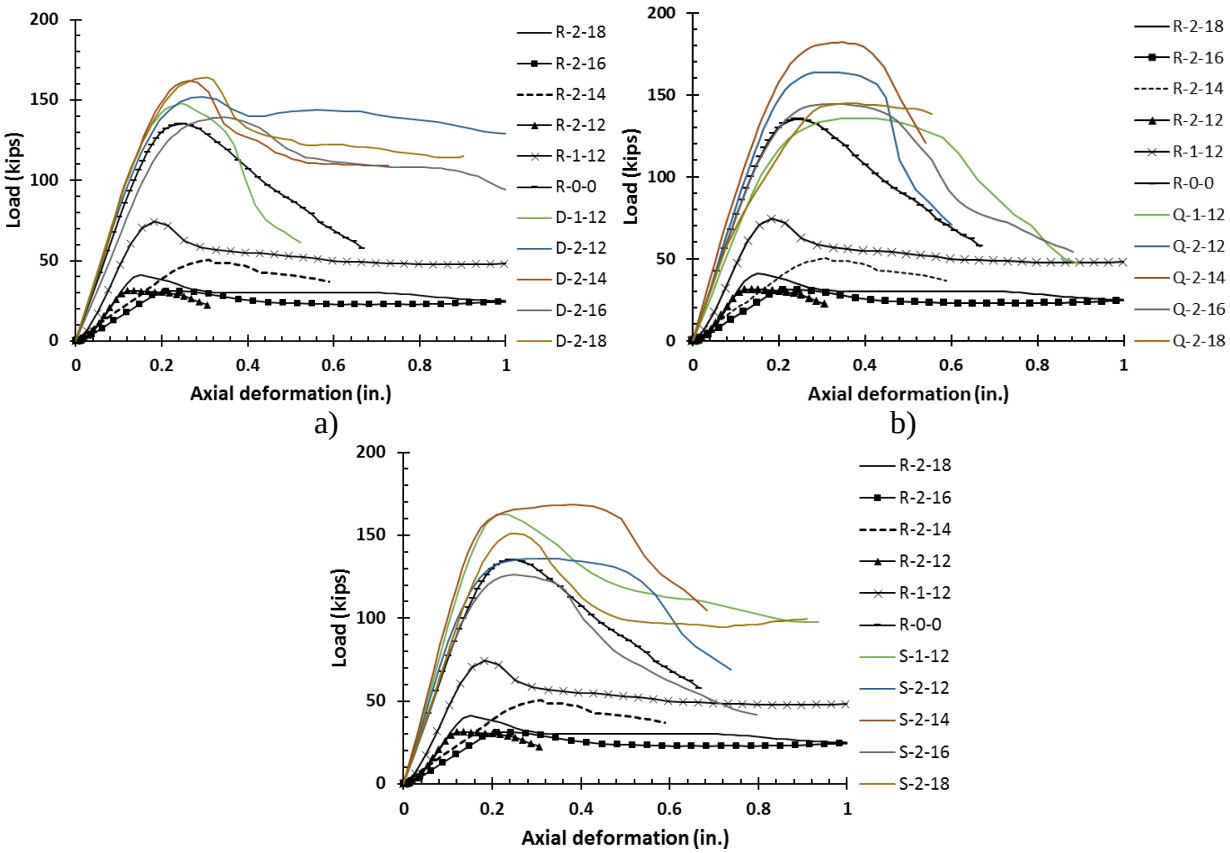

Figure 14**:** Load versus axial deformation for concentrically loaded piles, a) Densona, b) Pilemedic, c) Simpson

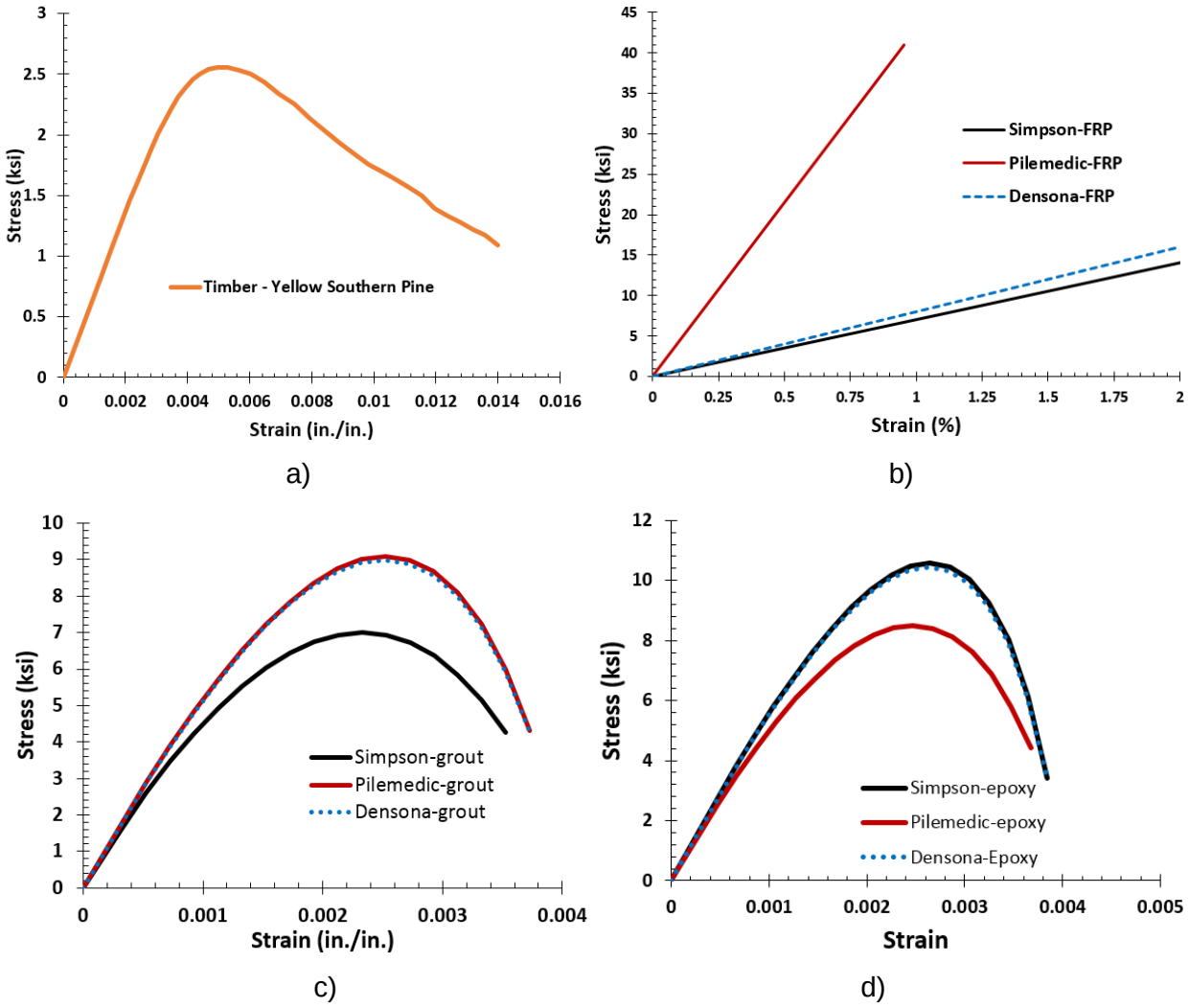

Figure 15. Stress-strain curves for a) wood, b) FRP, c) grout, d) epoxy

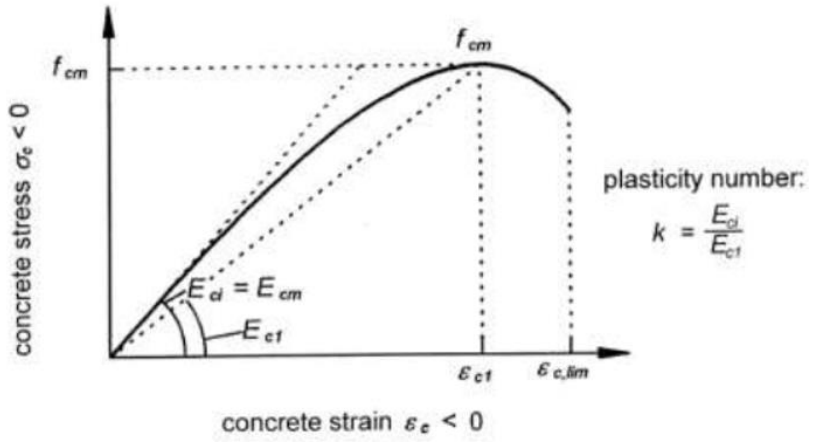

Figure 16. Schematic representation of stress-strain relation for uniaxial compression [27]

Table 4: Modules E_{ci}, E_{c1}, strains ε_{c1}, $\varepsilon_{c,lim}$ and plasticity number k for normal weight concrete [27]

Properties	Concrete Grade						
	C12	C20	C30	C40	C50	C60	C70
E_{ci} (GPa)	27.1	30.3	33.6	36.3	38.6	40.7	42.6
E_{c1} (GPa])	11.1	13.3	16.5	20.0	23.2	26.2	28.9
ε_{c1} (‰)	-1.8	-2.1	-2.3	-2.4	-2.5	-2.6	-2.7
$\varepsilon_{c,lim}$ (‰)	-3.5	-3.5	-3.5	-3.5	-3.4	-3.3	-3.2
k	2.44	2.28	2.04	1.82	1.66	1.55	1.47

The iterative procedure described in Figure 17 was used to obtain the predicted load versus deformation relationship for the repaired piles. The repaired pile was divided into three segments. Segment 1 represents the portion of the timber pile outside the repair. Segment 2 represents the portion of the timber pile inside the repair but before the tapered region, and segment 3 represents the portion of the repaired pile within the repair at the tapered region. The total deformation is calculated by adding the axial deformations in segments 1, 2 and 3. The axial deformation in segment 1 is calculated by assuming a strain and by multiplying strain with L1. Then, the assumed strain is used together with the stress-strain curve to obtain the corresponding stress in wood in Segment 1. This stress is multiplied with the area of Segment 1 to obtain the corresponding load (P). The axial deformation in segment 2 is calculated iteratively, by assuming a strain, entering the stress-strain curve for each material, calculating stress, calculating load by multiplying stress with the area of each material, and by comparing the summation of the axial loads in each material with the axial force calculated for Segment 1. If they match, no iteration is necessary and the assumed strain is correct. If not, then a different strain is assumed and the procedure is repeated until the load obtained for Segment 1 and the summation of loads in each material match. Once the solution converges, the axial deformation in segment 2 can be calculated by multiplying the strain with L2. The same procedure is repeated for segment 3 except that segment 3 is divided into five layers or more. Once the strain for each layer is obtained, it is expressed as a function of distance from the mid-height of the pile and integrated over the segment L3. Then, the axial deformations in each segment are added and the load P and total deformation Δ are stored. Finally, the entire procedure is repeated for a different level of strain in Segment 1 until the entire usable strain of the timber pile is exhausted.

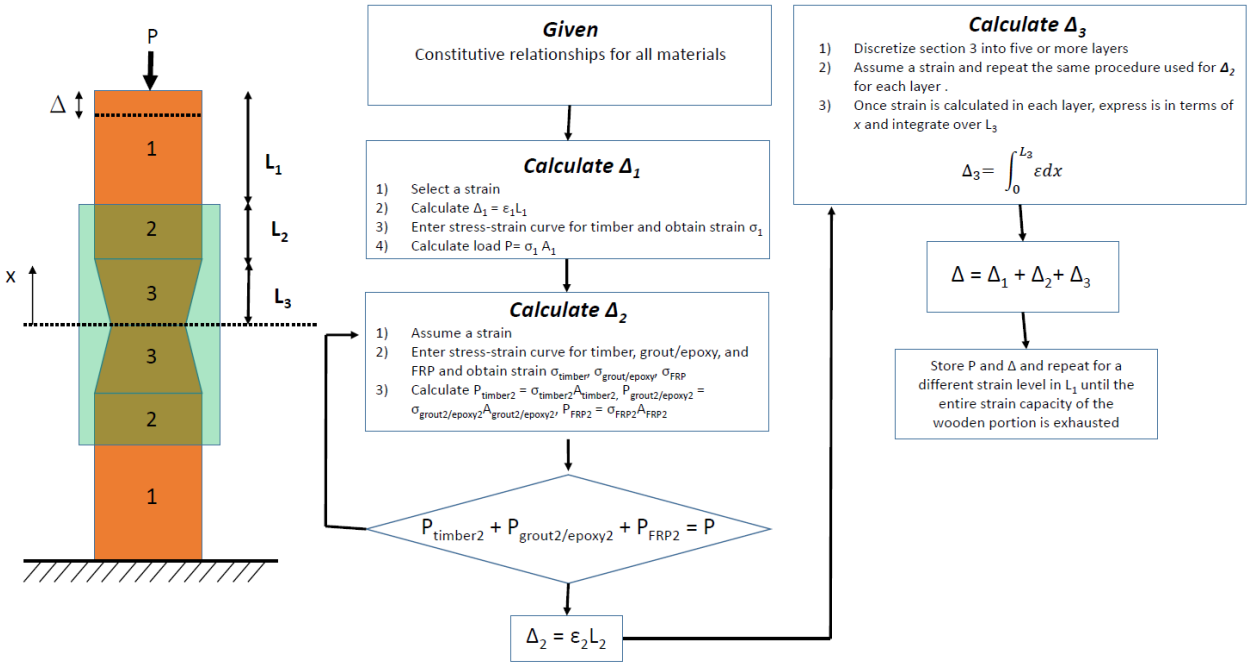

Figure 17. Prediction of load displacement curve

Figure 18 shows the comparison between predicted and measured load displacement curves for six repaired piles. In general the predicted response is slightly stiffer than the measured response. The difference between the measured and predicted responses for the piles repaired with Densona products is almost negligible. Also, the predicted and measured behaviors for S-1-12 are very similar with the exception that the measured peak load is slightly higher than the predicted peak load. The slight differences between the measured and predicted load displacement curves are attributed to the variability in wood material and as well as the assumed stress-strain curve for the infill grout/epoxy. In terms of peak loads, the average ratio between the measured and predicted values is 1.03 and the coefficient of variation is 7.68%. These results suggest that the adopted method for predicting the axial load versus deformation relationship yields reasonable results. An examination of the strain levels in the FRP, grout/epoxy, and timber in the repaired portion of the pile revealed that the behavior of the repaired portion remained linear elastic throughout the entire test. The timber portion outside the repaired region was the one that experienced loading in the inelastic branch of the stress-strain curve for timber. This was due to the fact that the material stiffness of the infill grout and epoxy was much higher than that of the wood material. Additionally, the cross-sectional area of the infill grout/epoxy was larger than that of the timber pile at any given cross-section in the repaired region.

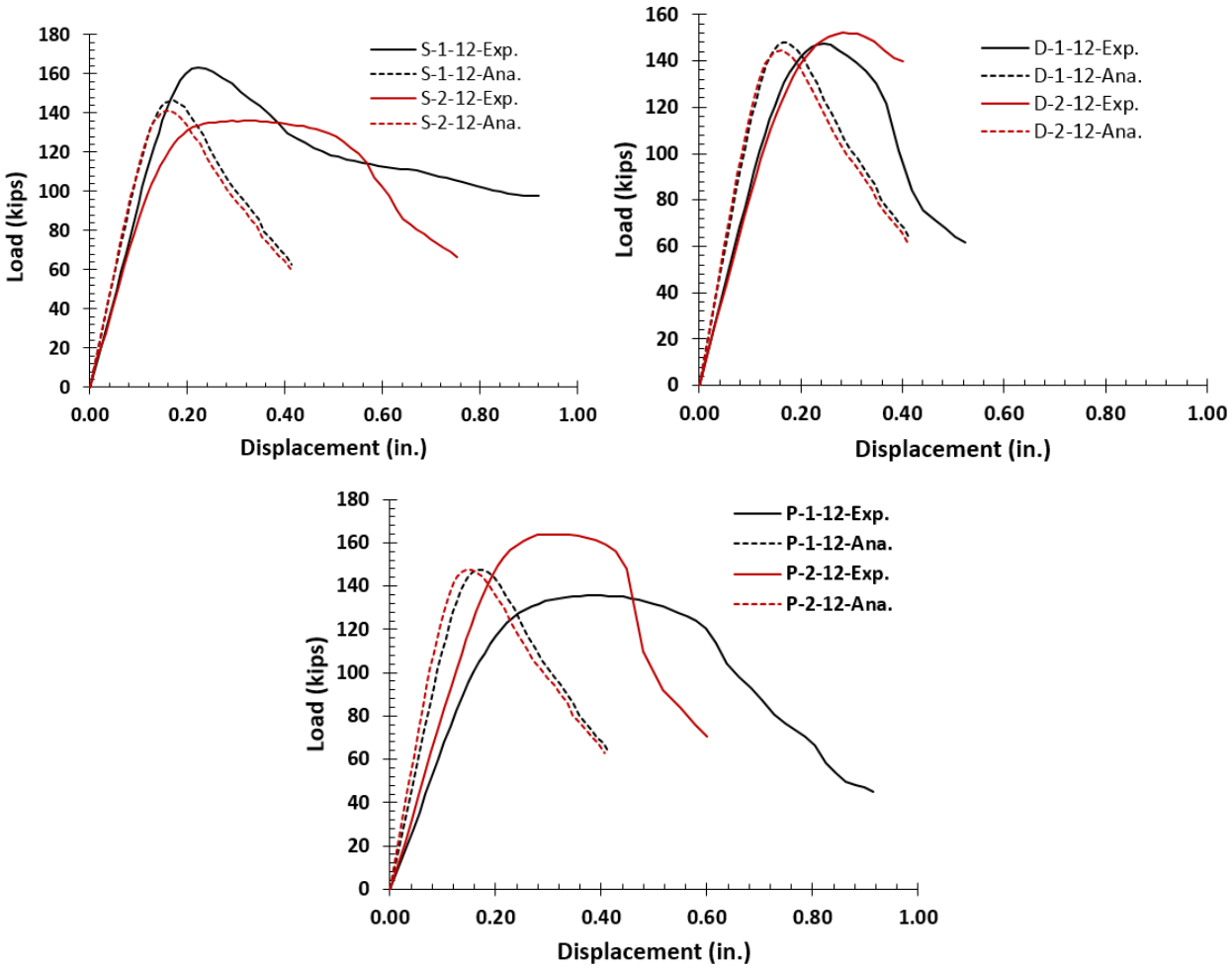

Figure 18. Comparison of measured and predicted load displacement curves

Table 5: Comparison of measured and predicted peak loads

Repaired Pile	Peak Load		Ratio $=P_m/P_p$
	Measured (P_m)(kips)	Predicted (P_p)(kips)	
S-1-12	162	146	1.11
S-2-12	136	141	0.96
D-1-12	147	147	1.00
D-2-12	151	144	1.05
P-1-12	135	147	0.92
P-2-12	163	147	1.11
		Average	1.03
		COV (%)	7.68

Figure 19 shows the breakdown of predicted load versus axial displacement at mid-height of repaired piles. This breakdown is provided for damage configuration X-2-12 for each repair technique. Figure 19 shows that at mid-height of the repaired pile essentially the entire

load is carried by the infill grout. The load supported by the timber, and FRP is negligible. The contribution of the FRP was intuitively expected to be negligible due to the small cross-sectional area of the FRP compared to the infill grout. Similarly, the area of the timber pile at mid-height is roughly eight times smaller than of the infill grout. Additionally, the stiffness of timber is approximately eight times smaller than that provided by the infill grout. The combined effects of a smaller cross-sectional area and smaller material stiffness led to a negligible contribution of the timber pile in terms of load carrying capacity at mid-height. A similar load break down was conducted for the layer at the intersection of segments L_2 and L_3. This is illustrated in Figure 20. Because the cross-sectional area of the timber pile in this segment is larger, its contribution to the load carrying capacity of the composite section increases. The contribution of the FRP shell remains negligible.

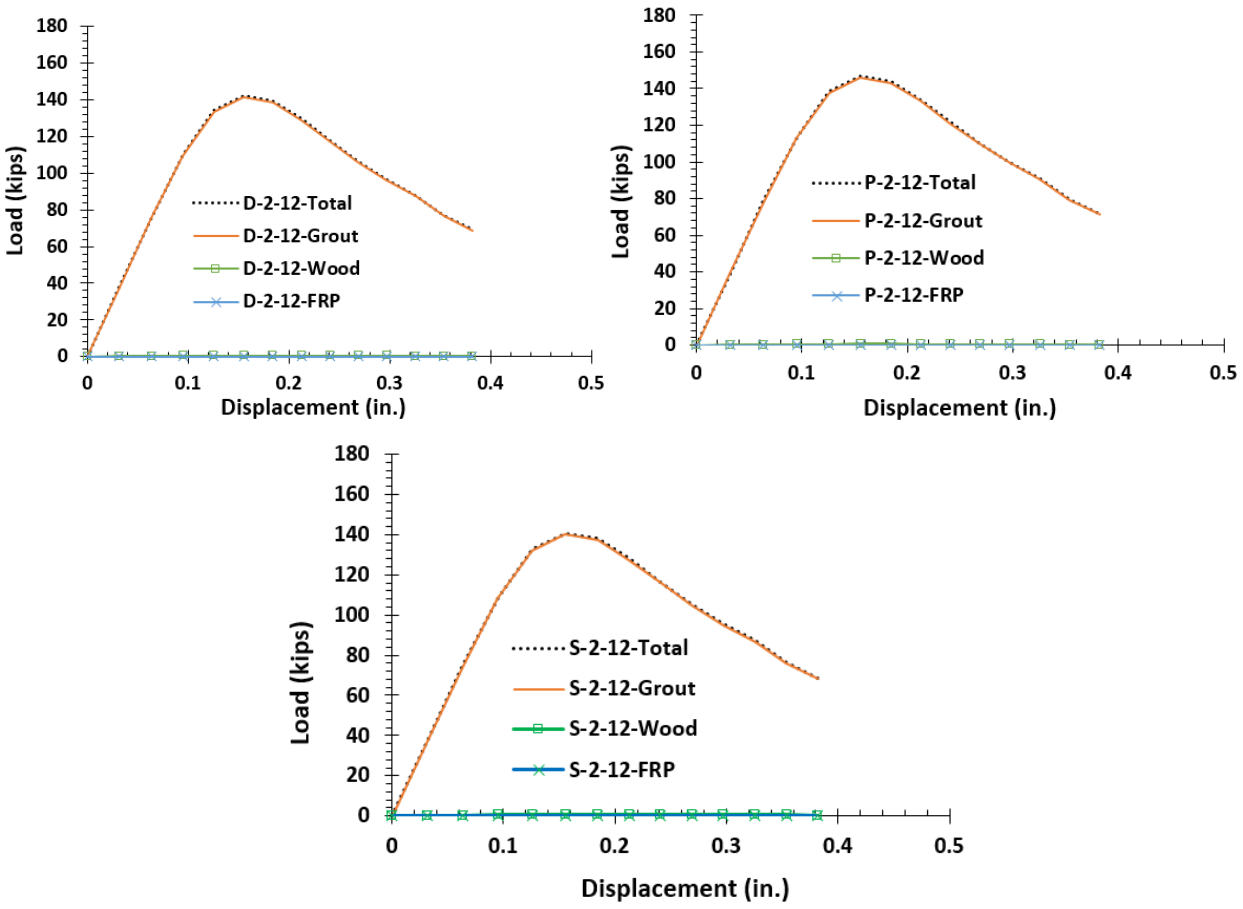

Figure 19. Break down of predicted load versus axial displacements for each component at mid-height of repaired pile

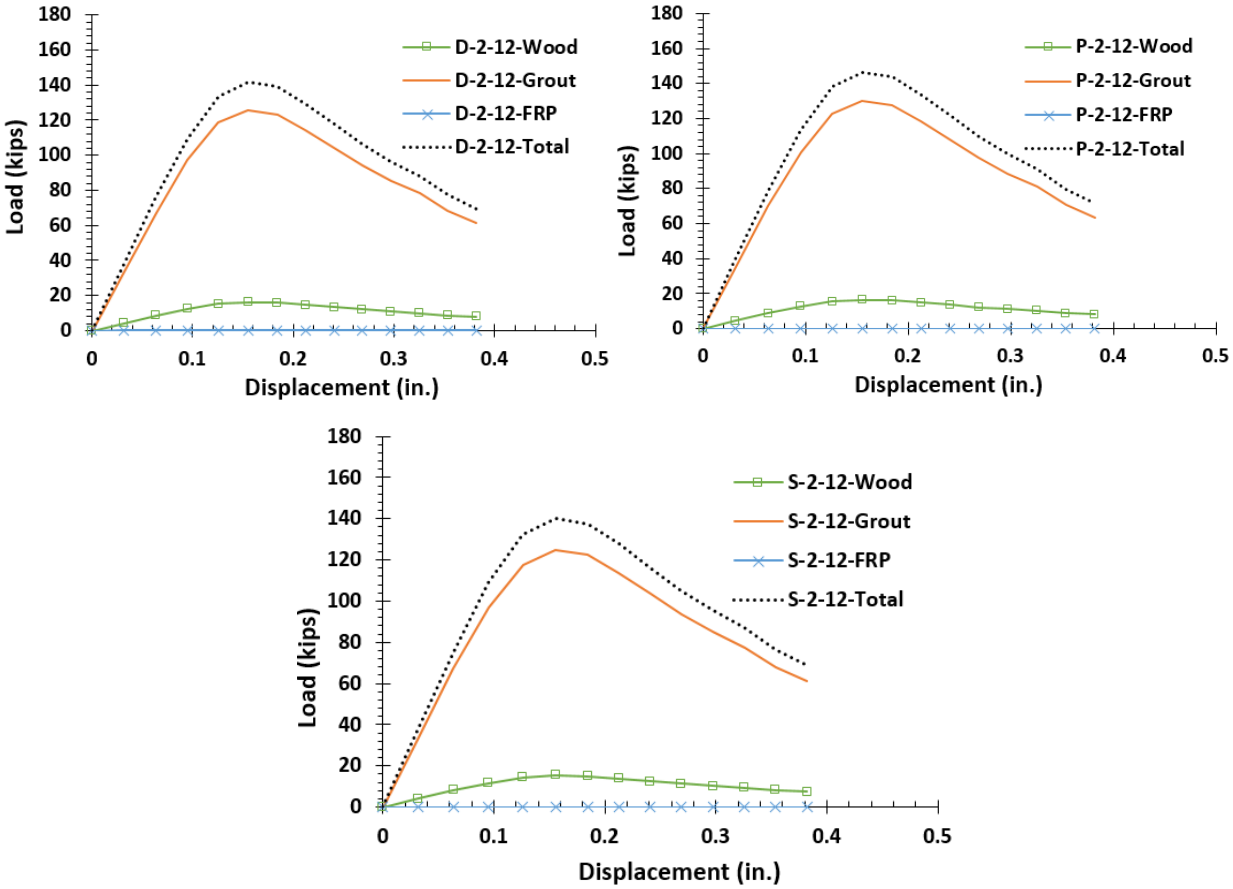

Figure 20. Break down of predicted load versus axial displacements for each component at intersection of segments L_2 and L_3 in the repaired pile

Figure 21 illustrates typical load versus strain curves for damaged piles with a 2 in. and 1 in. annular void (Figure 21a, Figure 21b). The minus sign indicates compression and the plus sign indicates tension. As expected, the vertically oriented strain gages are in compression and the horizontally oriented ones are in tension (circumferential strain). The vertical strains are higher than the hoop strains in both cases. The magnitude of vertical and hoop strains in the repaired pile with 1 in. annular void are several times larger than the strains in the repaired piles with a 2 in. annular void. This suggests that the FRP jacket is mobilized significantly more when the annular void is smaller. The greater mobilization of the FRP jacket in cases with smaller annular voids is due to the fact that a smaller volume of epoxy leads to a smaller axial stiffness and consequently larger strains. Figure 22 illustrates the mobilization of the FRP jacket in both cases. The capacity of the FRP shell provided by Denso North America in terms of ultimate tensile strength (F_{tu}), ultimate tensile strain (ε_{tu}) and modulus of elasticity (E) is 16 ksi, 2%, and 800 ksi, respectively. Simpson Strong Tie offers an FRP shell with similar properties (F_{tu} = 15

ksi, ε_{tu} = 2.14%, E = 700 ksi). The laminates produced by Pilemedic are over five times stiffer and over 2.5 times stronger than those produced by Densona and Simpson. However the ultimate tensile strain is less than half of that offered by Densona and Simpson. The ultimate tensile stress, ultimate tensile strain, and modulus of elasticity for Pilemedic laminates are F_{tu} = 41 ksi, ε_{tu} = 0.95%, E = 4297 ksi, respectively.

The maximum recorded vertical strain in the repaired pile with 1 in. annular void varies from 0.35% to 0.75% and the maximum horizontal strain is approximately 0.10%. For the repaired piles with a 2 in. annular void the vertical strain values are approximately 0.1% and horizontal strain values vary from 0.025% to 0.035%. In terms of structural utilization, less than 53% and 11% of the FRP shell strain capacity is used in piles with a 1 in. and 2 in. annular space, respectively. This suggest that as the annular void gets larger the primary function of the FRP shell is to serve as a stay in place form rather than provide circumferential confinement or any additional structural capacity.

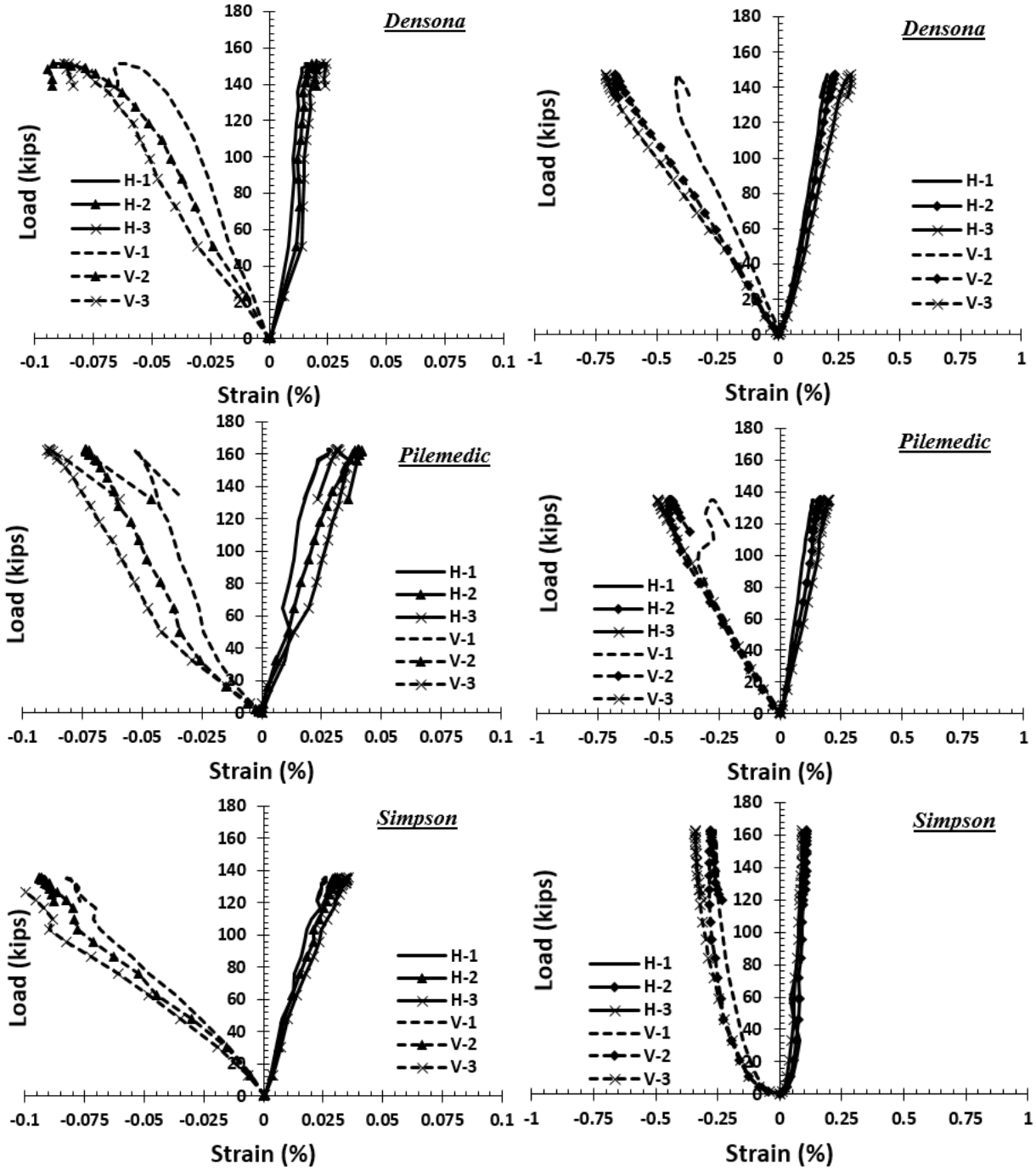

Figure 21. Load versus strain diagrams for concentrically loaded piles, a) typical diagram for specimens with 2 in. annular void, b) specimen with 1 in. annular void

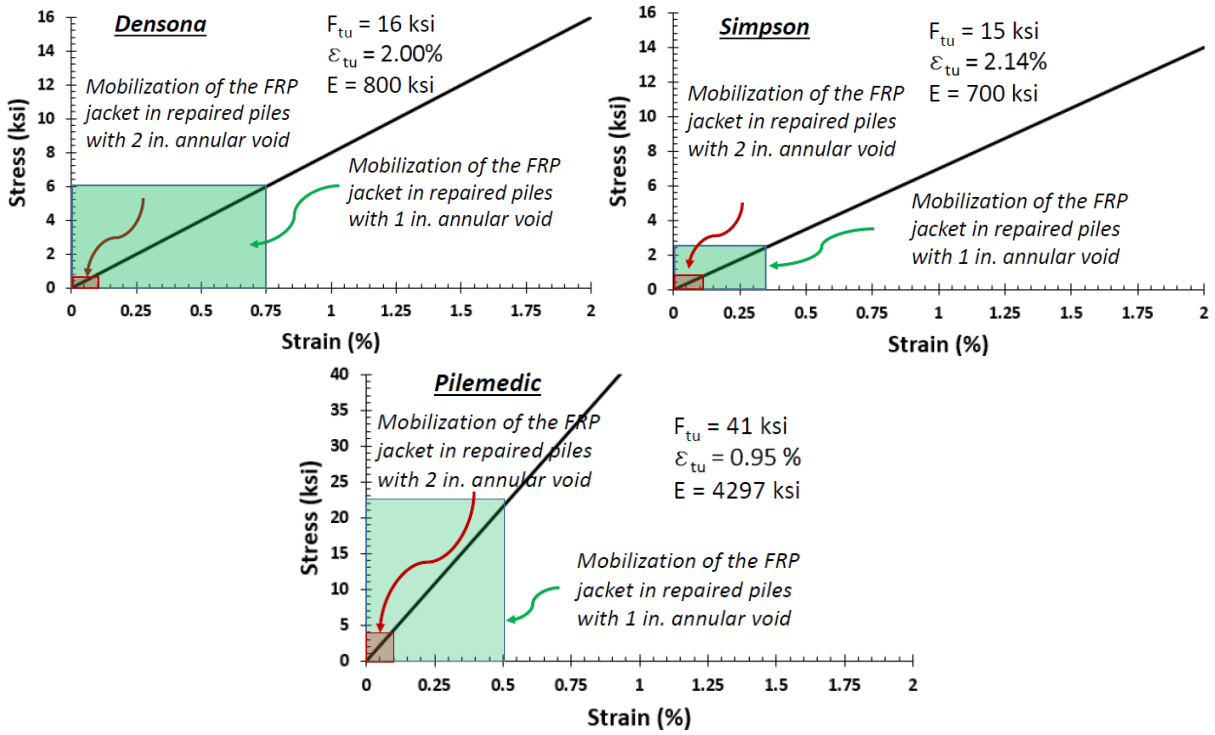

Figure 22**.** Stress-strain curve for FRP jacket and its mobilization based on the thickness of annular void for concentrically loaded piles

The measured load versus vertical strain curves were compared with predicted strains using the iterative procedure described in Figure 17. Figure 23 illustrates this comparison for the piles with damage configuration X-2-12. The piles were repaired with the three repaired techniques described earlier and the comparison was conducted for the relationship between load and vertical strain in strain gage V-3 (Figure 11). As described earlier, the iterative procedure assumes full composite action between all components and the similarity of load-strain curves shown in Figure 23 validates this assumption.

Figure 24 illustrates the load versus LVDT displacement for all repaired piles. As stated earlier, some relative displacement between the wooden portion of the pile and the repaired portion was expected due to the change in axial stiffness. The measured relative displacement in most cases was less than 0.08 in. The measured relative displacements at the top and bottom of the repair were generally similar and any differences are attributed to local defects either at the top or bottom portions outside the repair. The repaired piles were visually inspected for any potential slip at the pile-fill interface, however, no such slip was observed. This observation is consistent with the failure mode of the repaired piles, which featured a material failure in the wooden portion of the pile outside the repaired region. The measured relative

displacements were compared with the predicted difference between the axial displacement in L_1 and L_2 (see Figure 17). This comparison is illustrated in Figure 25. The measured response is stiffer than the predicted response because the measured response reflects only the difference in displacements between the points of attachments of the LVDT and clip angle. The predicted axial displacement is based on the difference between total displacements in segments L_1 and L_2. However, the fact that the predicted response, which was obtained under the assumption of full composite action between all three materials, is softer than the measured response, is another indication of the full composite behavior of the repaired piles until failure.

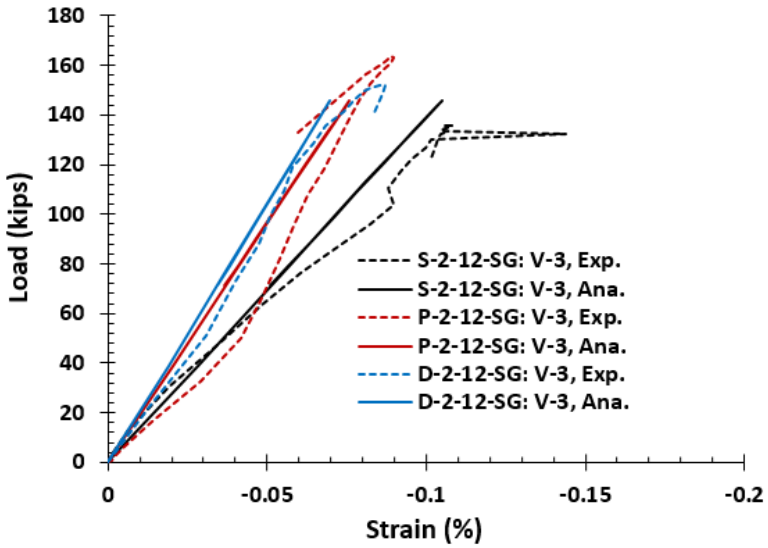

Figure 23. Comparison of measured and predicted load versus vertical strain curves

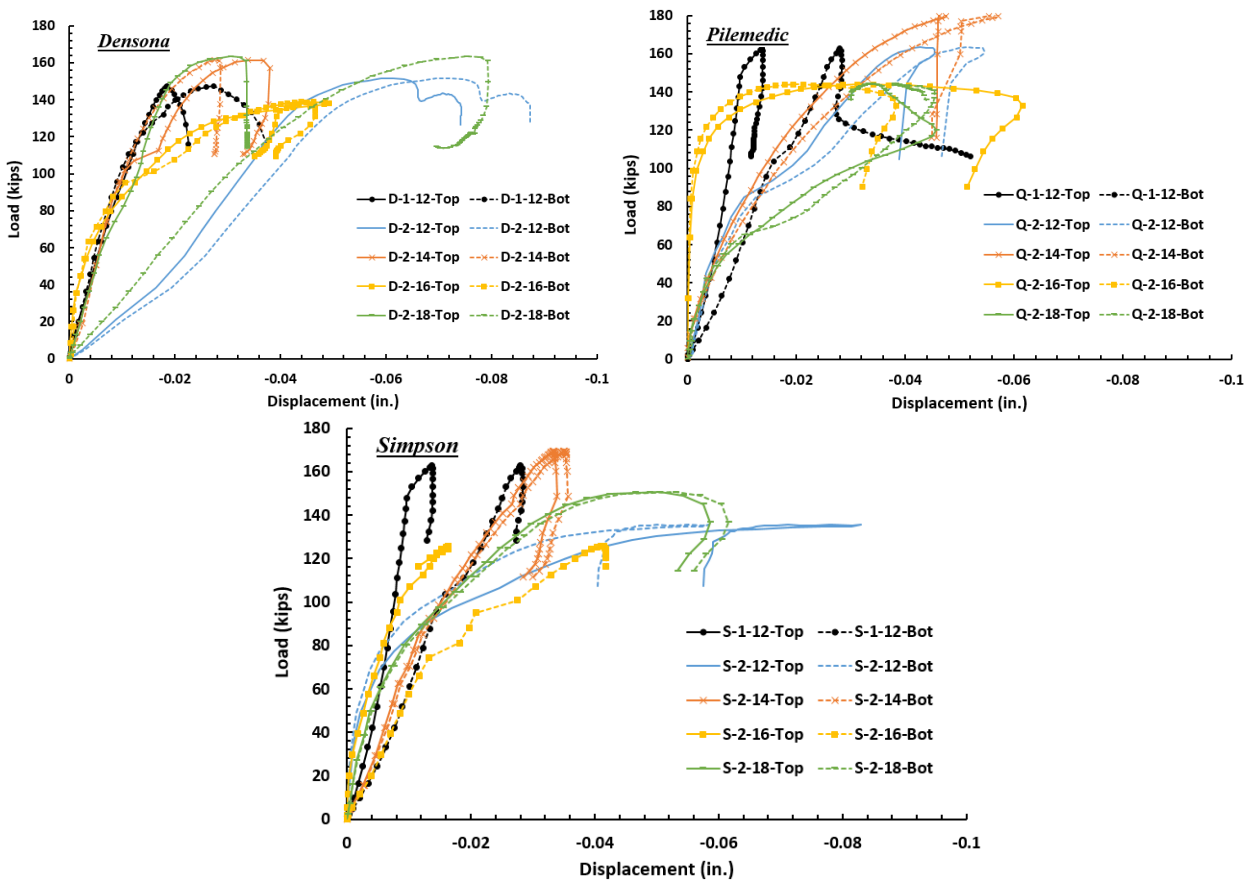

Figure 24**.** Load versus LVDT displacement for concentrically loaded piles

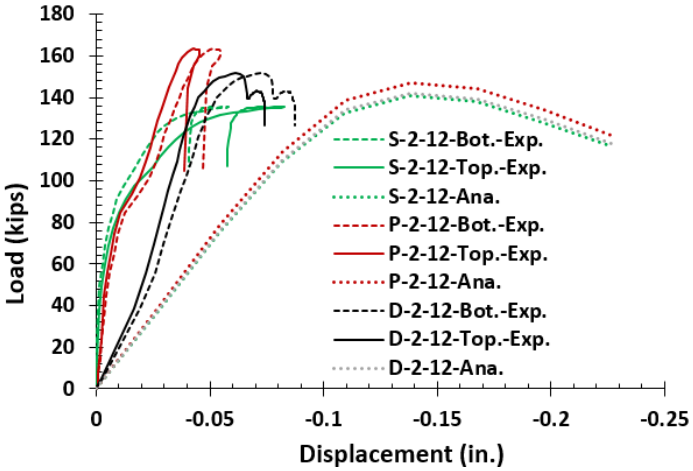

Figure 25. Comparison of measured load versus LVDT displacement with predicted load versus difference in axial displacements in L_1 and L_2

Axial Load Plus Bending Tests

A total of 21 tests were conducted on eccentrically loaded piles. As shown in Table 1, one test was conducted on an undamaged pile, five tests were conducted on damaged unrepaired piles featuring various damage configurations, and 15 tests (five for each repair technique) were conducted on damaged and repaired piles using the repair methods illustrated in Figure 6. The damage configuration in the damaged and repaired piles matched the damage configuration in the damaged and unrepaired piles so that the efficiency of the repair techniques could be evaluated. The goal was to compare the eccentric axial load capacities of damaged and repaired piles with those obtained from damaged unrepaired piles and the undamaged pile. The test on the undamaged pile was conducted to establish a baseline for undamaged capacity. The tests on damaged unrepaired piles were conducted to quantify the reduction in axial load capacity caused by the induced damage. Figure 26 illustrates the test setup for the eccentrically loaded piles featuring the same loading frame that was used for the axially loaded piles. The instrumentation was identical to that used for axially loaded piles. Three vertical strain gages denoted C1, C2, and C3 and three horizontal strain gages denoted H1, H2, and H3 were installed to measure vertical strain and circumferential strain, respectively. Two LVDTs were installed to measure any potential slip between the repaired and undamaged portion of the pile.

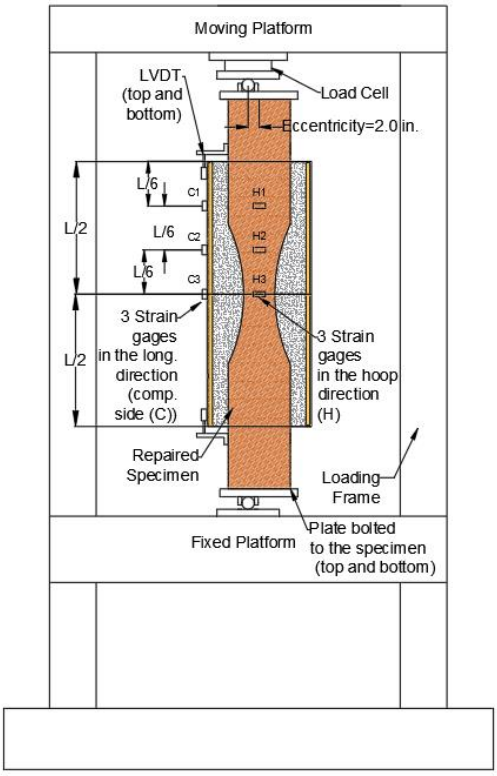

Figure 26. Test setup for eccentrically loaded piles

The piles were loaded at a 2.0 in. eccentricity at both ends. A steel plate was attached at each end of the pile using steel screws (Figure 27). This loading setup creates a uniform axial force and bending moment along the length of the pile. Figure 27 shows the configuration of the steel plate and bolts. The eccentric failure load was estimated using Eq. 2 by assuming a linear elastic behavior and by setting the maximum compressive stress equal to the average compressive stress obtained from the 21 concentrically loaded piles. This average compressive stress was 2.625 ksi. While the behavior of the reference undamaged pile tested under concentric loads was nonlinear, this was done to have a general idea about the eccentric failure load and to design the steel plate timber pile connection. The eccentric failure load *P* was back calculated and is equal to 51 kips. Then, Eq. 3 was used to calculate the maximum tensile stress and consequently the maximum estimated tensile force so that the connection could be designed accordingly. The maximum tensile stress is 0.83 ksi and the maximum tensile force is 8.47 kips. The maximum tensile force was conservatively calculated by multiplying the maximum tensile stress with the area of the pile in tension. Eq. 4 is used to calculate the portion of the timber pile that is in compression. Eq. 5 was used to calculate the withdrawal resistance of a single steel screw [28]. The steel screws that were used to connect the steel plate to the timber pile were 0.5 in. in diameter and had a length of penetration for the threaded part equal to 6.5 in. The withdrawal resistance according to Eq.5 provided in the “Wood Handbook, Wood as an Engineering Material” [28] is 12.6 kips/bolt. Figure 27 shows that the layout of bolts as well as the portion of the pile that is in tension. There is a total of three screws that are in tension and therefore the total withdrawal capacity is 37.8 kips, which is higher than the total tensile force calculated as 8.47 kips.

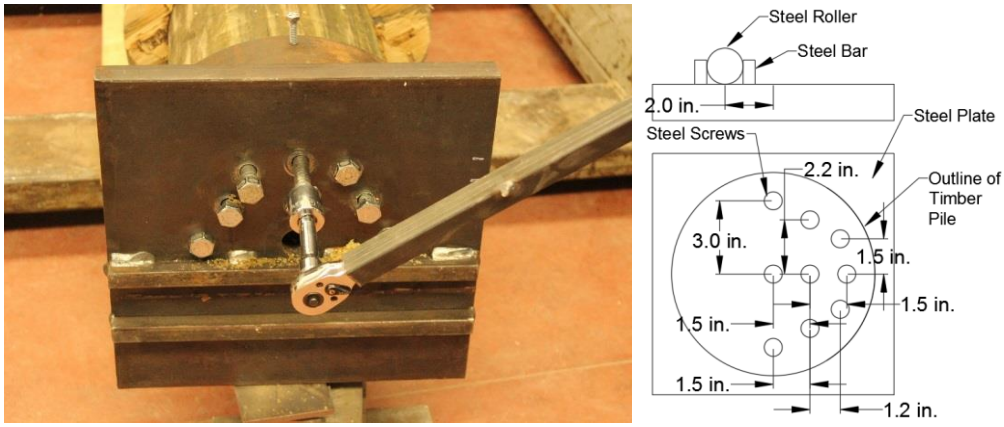

Figure 27. Connection between steel plate and timber pile

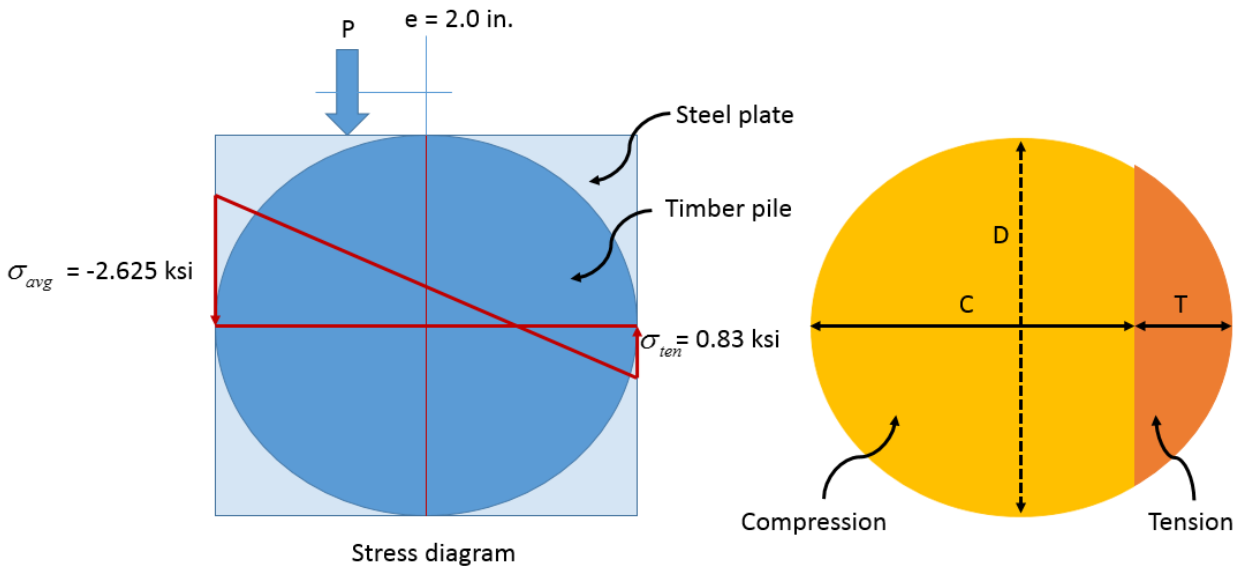

Figure 28. Calculations of compressive and tensile stresses regions assuming linear elastic behavior

$$\sigma_{com} = \frac{P}{A} + \frac{Pey}{I} \quad (2)$$

$$\sigma_{ten} = \frac{P}{A} - \frac{Pey}{I} \quad (3)$$

where

P = estimated failure load (kips)

A = area of timber pile (in^2)

e = eccentricity of axial load (in.) = 2.0 in.

y = distance from centroid to fiber of interest (in.)

I = moment of inertia of timber pile (in^4)

σ_{com} = compressive stress (ksi)

σ_{ten} = tensile stress (ksi)

$$C = \frac{D}{2} + \frac{I}{Ae} \quad (4)$$

C = depth of compression block (in.)

D = diameter of pile (in.)

$$P_{bolt} = 8100 G^{\frac{3}{2}} D^{\frac{3}{4}} L \quad (5)$$

where

P_{bolt} = maximum withdrawal load (lb) = 12.6 kips/bolt

D = diameter of bolt (in.) = 0.5 in.

G = specific gravity of the wood = 0.55 (Southern Pine)

L = length of penetration of the threaded part (in.) = 6.5 in. (actual bolt length = 10 in.)

Results of Axial Load Plus Bending Tests

Table 6 provides a summary of peak loads for all eccentrically loaded piles. The failure load for the reference undamaged pile was 68 kips and the failure loads for damaged and repaired piles vary from 64 kips to 81 kips. The 2 in. eccentricity causes a 45%-51% reduction in peak loads compared to those obtained for concentrically loaded piles. The peak loads for the repaired piles were compared with the peak loads for the undamaged pile as well as the peak loads for the damaged unrepaired piles that featured the same damage configuration. The ratios between the peak loads of repaired piles and damaged unrepaired piles varied from 3.30 to 6.75, which means that the repairs can increase the capacity of damaged piles from 230% to 575%. The average ratio was 5.43 and the coefficient of variation was 21.56%. The ratios between the peak loads of the repaired piles and the reference undamaged pile varied from 0.94 to 1.19. The average ratio was 1.09 and the coefficient of variation was 8.19%. The failure in all cases took place outside of the repaired region and the failure mode was a material failure of the wood. Only in three cases were the ratios smaller than 1.0 (0.94 and 0.97) and this is attributed to the variability in wood material rather than the efficiency of the repair.

Table 6: Failure loads of all eccentrically loaded specimens

Specimen No.	Length of damage (in.)	Depth of damage (in.)	Failure Load (kips)	Ratio = Repaired/Baseline	
				Ratio 1 = Repaired/Undamaged	Ratio 2 = Repaired/Damaged
R-0-0	0	0	68	NA	NA
R-1-12	12	1	20	NA	NA
R-2-12	12	2	12	NA	NA
R-2-14	14	2	14	NA	NA
R-2-16	16	2	12	NA	NA
R-2-18	18	2	13	NA	NA
D-1-12	12	1	69	1.01	3.45
D-2-12	12	2	80	1.18	6.67
D-2-14	14	2	70	1.03	5.00
D-2-16	16	2	80	1.18	6.67
D-2-18	18	2	70	1.03	5.38
P-1-12	12	1	73	1.07	3.65
P-2-12	12	2	81	1.19	6.75
P-2-14	14	2	77	1.13	5.50
P-2-16	16	2	64	0.94	5.33
P-2-18	18	2	80	1.18	6.15
S-1-12	12	1	66	0.97	3.30
S-2-12	12	2	76	1.12	6.33
S-2-14	14	2	81	1.19	5.79
S-2-16	16	2	77	1.13	6.42
S-2-18	18	2	66	0.97	5.08
			Average	**1.09**	**5.43**
			COV (%)	**8.19**	**21.56**

Figure 29 illustrates the failure mode in the undamaged pile as well as damaged unrepaired piles. The failure in the undamaged pile occurred at the ends and featured wood crushing and longitudinal cracking. The failure in all damaged unrepaired piles occurred at mid-height in the region that featured the smallest cross-section of the pile. The mode of failure was wood crushing. Figure 30 illustrates the typical failure mode for the repaired piles. For each repair technique the failure of the pile with a 1 in. damage depth and a typical failure for the piles with a 2 in. damage depth is shown. In general the failure mode featured a compression failure in the form of wood crushing. Two out of the 15 repaired piles featured screw pullouts, which was observed during the removal of the steel cap after the completion of the test. The repaired piles that featured screw pullouts were P-1-12 and D-2-18. While it is not clear at which loading stage the screws pulled out from the two piles, an examination of the peak load for P-1-12 and D-2-18 suggests that screw pullout must have occurred after the peak load was achieved sometime during the descending branch in the load displacement curve. The peak loads for P-1-12 and D-2-18 were 73 kips and 70 kips, respectively, which is between the range observed for the other piles (64 kips to 81 kips). The two screw pullout events are attributed to local defects in the wood at the connection region as well as damage in the tension zone after the peak load was achieved.

Figure 29. Testing of undamaged and damaged-unrepaired piles loaded eccentrically

Figure 30: Testing of eccentrically loaded repaired timber piles and illustration of failure mode

Figure 31 illustrates the load versus axial deformation of all eccentrically loaded piles. The capacity of the repaired piles is several times larger than that for similarly damaged unrepaired piles. Additionally, for most of the cases the capacity of the repaired piles is slightly larger than that of the undamaged reference pile. Also, the stiffness of the repaired piles is higher than that of the undamaged reference pile. This is due to the fact that the infill grout and epoxy is stiffer that the wood and therefore increases slightly the overall stiffness of the pile.

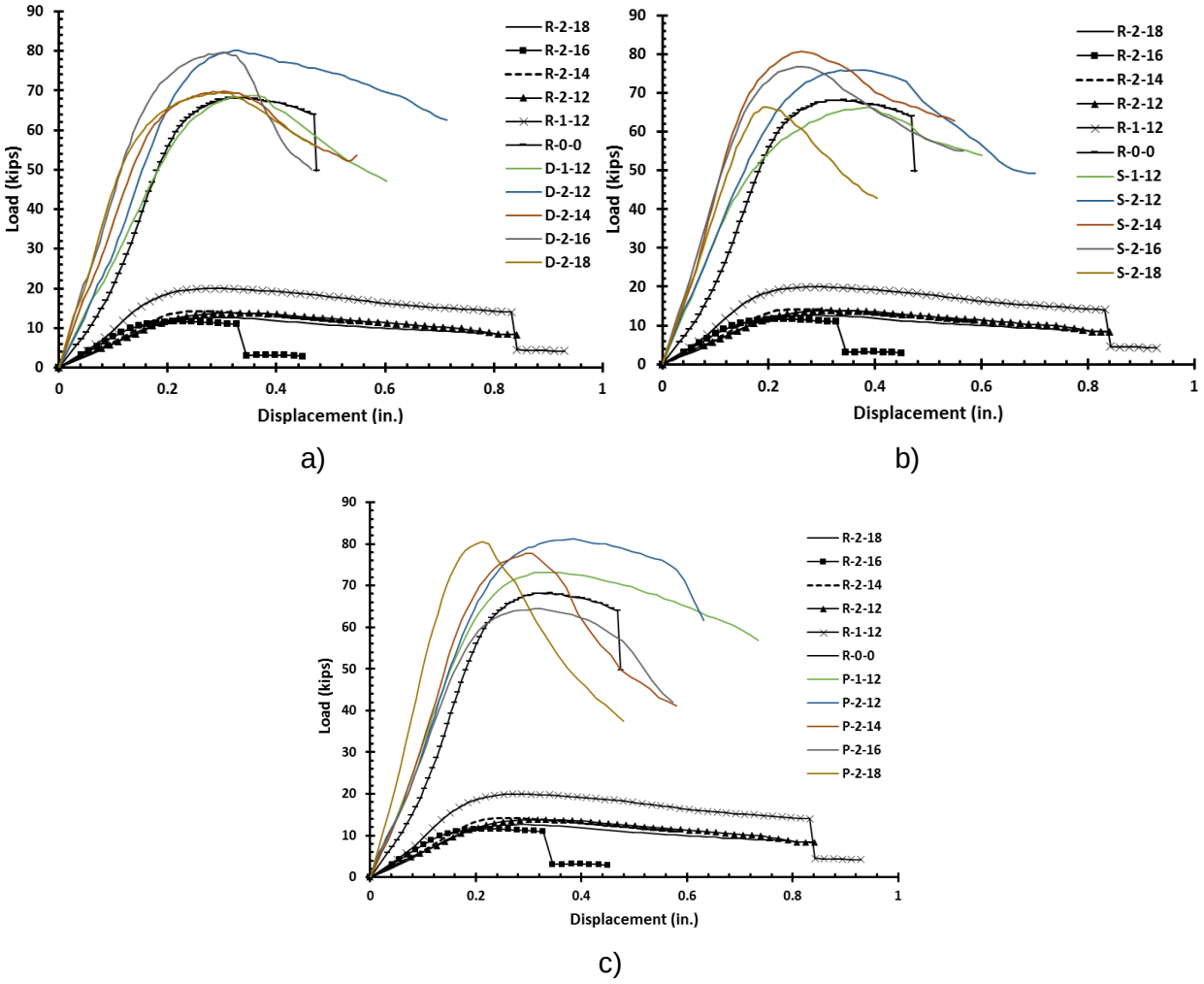

Figure 31. Load versus axial deformation for eccentrically loaded piles, a) Denso North America, b) Simpson Strong Tie, c) Pilemedic

Figure 32 illustrates typical load versus strain curves for damaged piles with a 2 in. and 1 in. annular void (Figure 32a, Figure 32b). The minus sign indicates compression and the plus sign indicates tension. As expected, the vertically oriented strain gages are in compression and the horizontally oriented ones are in tension (circumferential strain). The vertical strains are higher than the circumferential strains in both cases. The magnitude of vertical and circumferential strains in the repaired pile with 1 in. annular void are several times larger than the strains in the repaired piles with a 2 in. annular void. This suggests that the FRP jacket is mobilized significantly more when the annular void is smaller. The greater mobilization of the FRP jacket in cases with smaller annular voids is due to the fact that a smaller volume of epoxy leads to a smaller axial and flexural stiffness and consequently larger strains. Figure 33 illustrates the mobilization of the FRP jacket in both cases. The maximum recorded vertical

strain in the repaired pile with 1 in. annular void varies from 0.35% to 0.80% and the maximum circumferential strain is approximately 0.15%. For the repaired piles with a 2 in. annular void the vertical strain values vary from 0.05% to 0.15% and horizontal strain values vary from 0.01% to 0.04%. This suggest that as the annular void gets larger the primary function of the FRP shell is to serve as a stay in place form rather than provide circumferential confinement or any additional structural capacity.

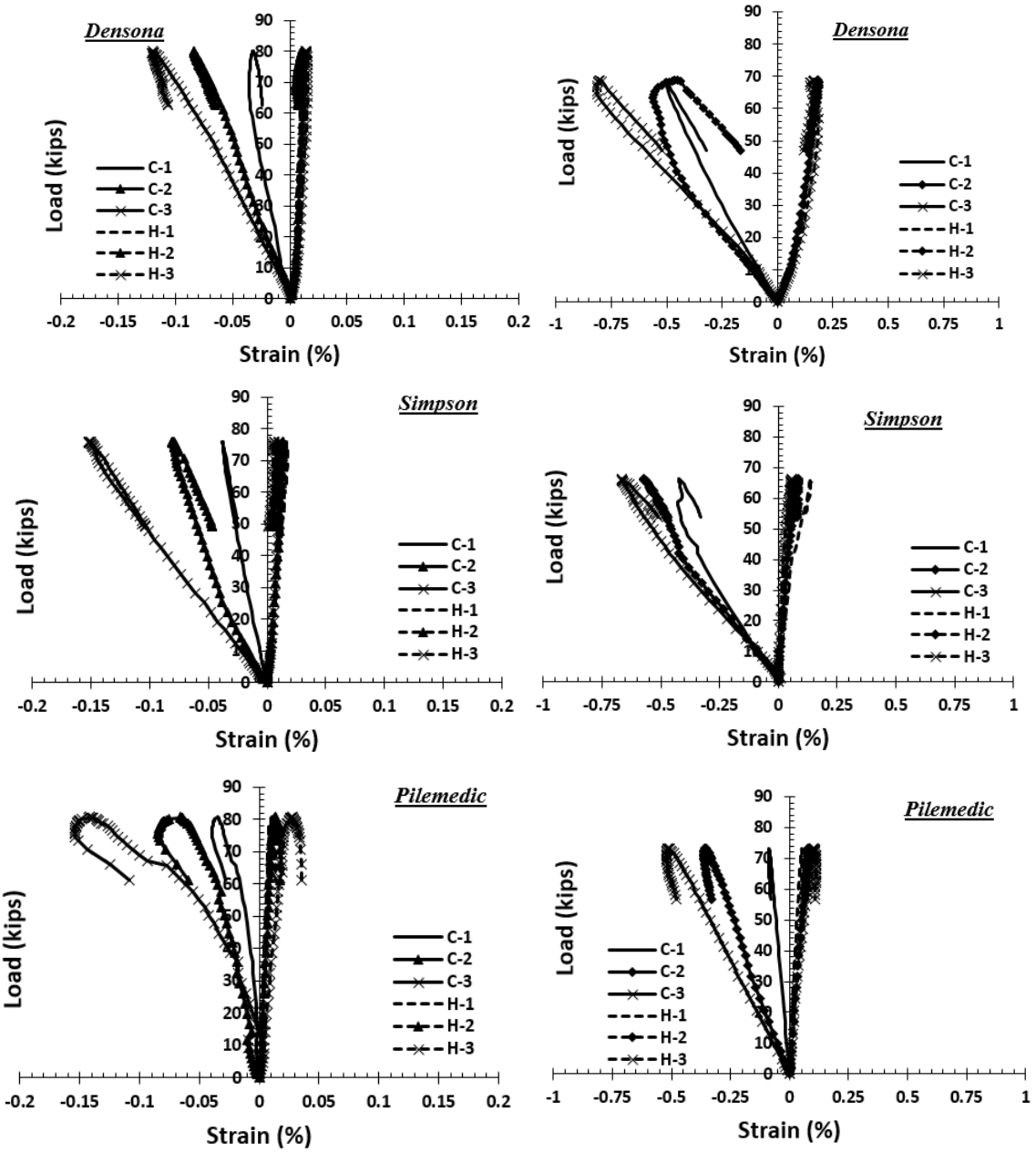

a) b)

Figure 32. Typical load versus strain diagrams for eccentrically loaded piles, a) specimens with 2 in. annular void, b) specimens with 1 in. annular void

Figure 33 illustrates the mobilization of the FRP jacket in both cases. The maximum measured strains in the piles with 1 in. annular void repaired with Densona and Simpson products vary from 0.75% to 0.80%. The ultimate strain capacity of the FRP shells in both cases is 2%. As a result, less than or equal to 40% of the capacity of the FRP shell is being utilized. The maximum measured strains in the piles with 1 in. annular void repaired with Pilemedic products are approximately 0.55%, which is less than the 0.95% ultimate strain capacity of the shell. Also, in this case only less than 60% of the capacity of the FRP shell is being utilized. The mobilization of the FRP shell for piles with a 2 in. annular void reduces significantly. In this case the measured strains for piles repaired with Densona and Simpson products vary from 0.10% to 0.15%, which is less than or equal to 7.5% of the capacity of the FRP shell. The measured strains in piles repaired with Pilemedic products were approximately 0.15%, which is equal to 16% of the capacity of the FRP shell. This suggests that as the annular void gets larger the primary function of the FRP shell is to serve as a stay in place form rather than provide circumferential confinement or any additional structural capacity.

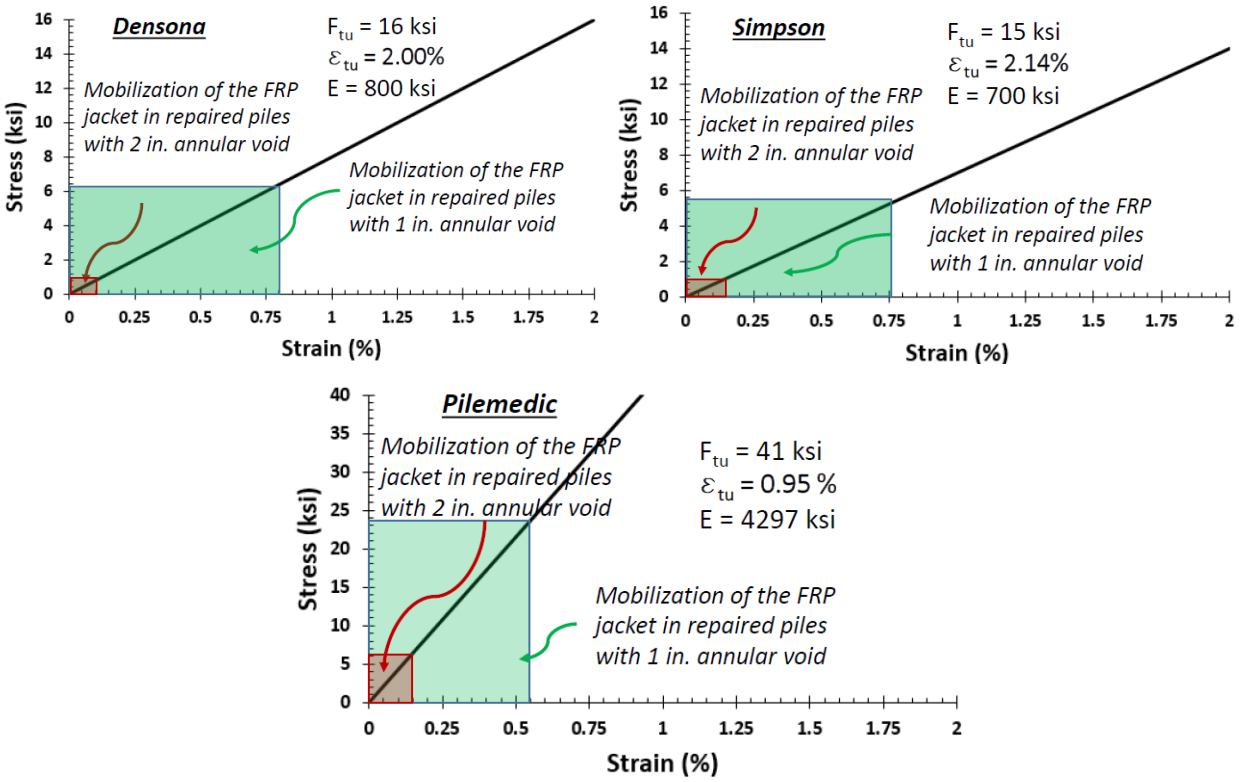

Figure 33. Stress-strain curve for FRP jacket and its mobilization based on the thickness of annular void for eccentrically loaded piles

Figure 34 illustrates the load versus LVDT displacement for all repaired piles. Some relative displacement, between the wooden portion of the pile and the repaired portion was expected due to the change in axial and flexural stiffness. The measured relative displacement was less than 0.07 in. The measured relative displacements at the top and bottom of the repair were generally similar and any differences are attributed to local defects either at the top or bottom portions outside the repair. The repaired piles were visually inspected for any potential slip at the pile-fill interface, however, no such slip was observed. This observation is consistent with the failure mode of the repaired piles, which generally featured a material failure in the wooden portion of the pile outside the repaired region.

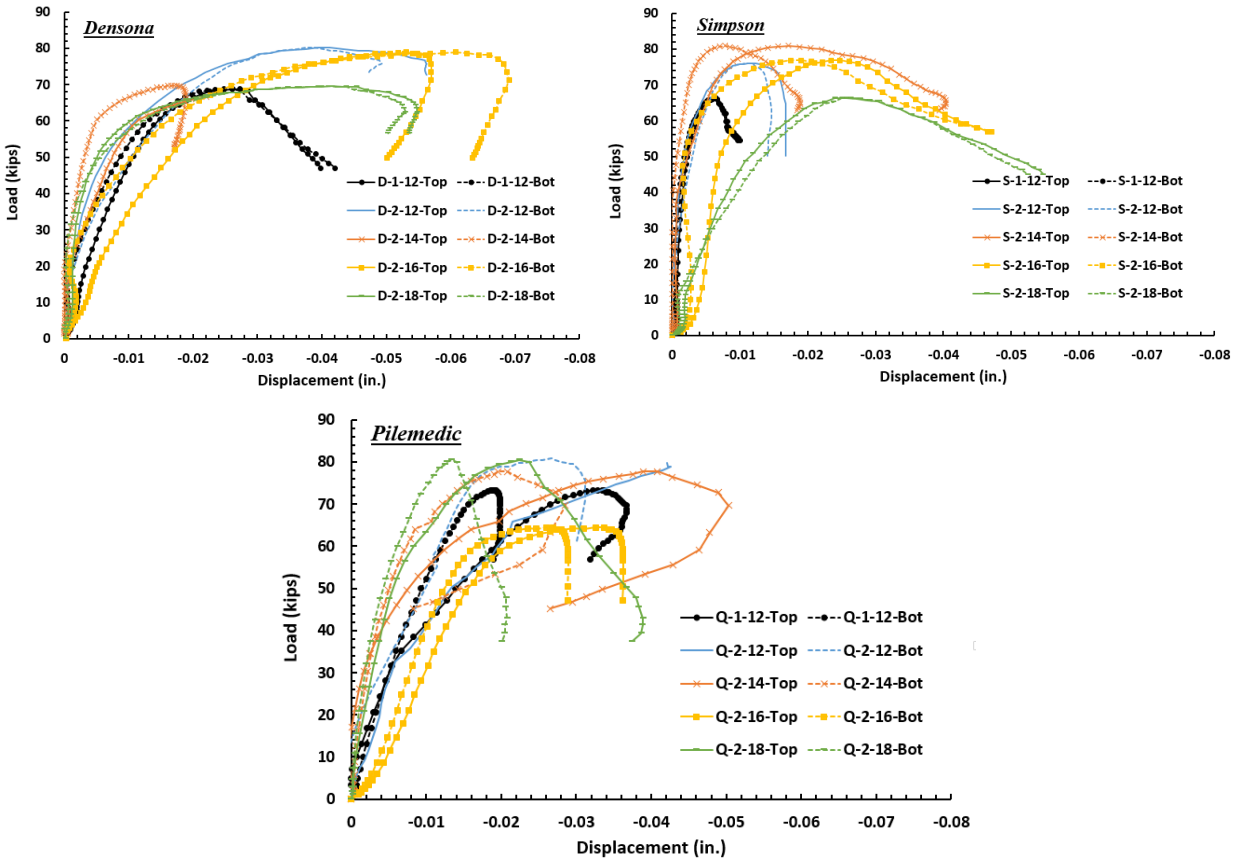

Figure 34. Load versus LVDT displacement for eccentrically loaded piles

CONCLUSIONS AND RECOMMENDATIONS

A total of 42 tests were conducted on undamaged, damaged, and repaired timber piles to characterize their behavior under concentric and eccentric loads. The repaired piles featured a FRP jacket, an underwater epoxy or grout fill and in some cases carbon fiber reinforcement between the FRP jacket and the timber pile. The repair materials are commercially available and were provided by Denso North America, Simpson Strong Tie and Pilemedic.

The repaired piles exhibited concentric axial load capacities that were not only in excess of those measured for the damaged piles but also surpassed the axial capacity of the reference undamaged pile regardless of which repair technique was used. The concentric load capacity of the damaged piles was increased by 82% to 420% by repairing them with FRP composites. Additionally, the original concentric load capacity of the undamaged pile was typically enhanced as a result of the repair with the exception of one pile. Similarly, the eccentric load capacity of the damaged piles was increased by 230% to 575% by repairing them with FRP composites regardless of the repair technique. The original eccentric load capacity of the undamaged piles was typically enhanced as well with the exception of three piles for which the eccentric load capacity was slightly lower than that measured for the damaged pile. In general, the capacity of the repaired piles may be based on the wooden portion of the pile outside of the repair region if one of the repair techniques investigated in this study is adopted. A method was presented to predict the axial load versus axial deformation relationship for concentrically loaded repaired piles and it was shown that it leads to reasonable results given the variability in the wood material.

Strain gage measurements indicated that the FRP shell is mobilized more when the annular void is smaller. For 1 in. annular voids the mobilization of the FRP shell in terms of strains was less than 60% of the ultimate strain and for 2 in. annular voids it was less than 16% of the ultimate strain. The lower mobilization of the FRP shell for larger annular voids is attributed to the fact that a larger annular void results in an increased axial and flexural stiffness in the repaired portion of the pile, which leads to smaller strains.

Small relative displacements were recorded between the wooden portion of the pile and the repaired portion due to differences in axial and flexural stiffness between these two components. No slip was observed at the pile-fill interface and all failures modes featured a material failure in the wooden portion of the pile outside the repair.

All investigated repair techniques are efficient and can be used to rehabilitate deteriorated piles in terms of concentric and eccentric load capacities.

REFERENCES

[1] Mohammadi, A., Gull, J. H., Taghinezhad, R., and Azizinamini, A. (2014), “Assessment and Evaluation of Timber Piles Used in Nebraska for Retrofit and Rating”, Florida International University, Final Report to Nebraska Department of Roads, April.

[2] Reynolds, T.N. (2003). “Timber Pile Foundations”, BRE Digest 479, BRE Construction Division, BRE Bookshop, London, UK.

[3] Simpson Strong-Tie (2015) strongtie.com/rps

[4] Koppers. (2010). “Timber Pile Life Expectancy Guide”, Koppers Wood Products Pty Ltd, North Sydney, NSW.

[5] Tumialan, G.Z., Konicki, W., Westover, P., Vatovec, M. (2013). “Untreated Submerged Timber Pile Foundations Part 1: Understanding Biodegradation and Compressive Strength”, December 2013, Structure Magazine, NCSEA/CASE/SEI, C^{3}Ink, Reedsburg, WI.

[6] Tumialan, G.Z., Konicki, W., Westover, P., Vatovec, M. (2014). “Untreated Submerged Timber Pile Foundations Part 2: Estimating Remaining Service Life”, January 2014, Structure Magazine, NCSEA/CASE/SEI, C^{3}Ink, Reedsburg, WI.

[7] Vatovec, M., Kelley, P. (2007). “Biodegradation of Untreated Wood Foundation Piles In Existing Buildings Part 1- Investigation”, June 2007, Structure Magazine, NCSEA/CASE/SEI, C^{3}Ink, Reedsburg, WI.

[8] Vatovec, M., Kelley, P. (2007). “Biodegradation of Untreated Wood Foundation Piles In Existing Buildings Part 2- Deterioration Mechanisms”, September 2007, Structure Magazine, NCSEA/CASE/SEI, C^{3}Ink, Reedsburg, WI.

[9] Vatovec, M., Kelley, P. (2007). “Biodegradation of Untreated Wood Foundation Piles In Existing Buildings Part 3 – Remedial Options”, December 2007, Structure Magazine, NCSEA/CASE/SEI, C^{3}Ink, Reedsburg, WI.

[10] Goodell, B., Nicholas, D., and Schultz, T. (2003). *Wood deterioration and preservation: Advances in our changing world*, American Chemical Society Series, Oxford University

Press, New York.

[11] Lopez-Anido, R., Michael, A. P., and Sandford, T. C. (2004a). “Fiberreinforced polymer composite-wood pile interface characterization by push-out tests.” *J. Compos. Constr.*, 8(4), 360–368.

[12] Avent, R.R., Gopu, V.K.A. (1997). “Effect of Incipient Decay in Compressive Strength and Stiffness of Timber Piles”, Final Report, December 1997, Louisiana Transportation Research Center, Baton Rouge, LA.

[13] Gopu, V., Avent, R. (2012). “Effect of Incipient Decay in Compressive Strength and Stiffness of Timber Piles”, World Conference on Timber Engineering, July 16-19, 2012, Auckland, NZ.

[14] Baileys, R.T. (1995). “Timber structures and the marine environment”, *Ports ’95*, 703–710.

[15] U.S. Navy. (1987). *Polyvinyl chloride (PVC) wraps reduce the cost of maintaining timber piling*, Naval Civil Engineering Laboratory, Port Hueneme, Calif.

[16] Lopez-Anido, R., Michael, A.P., Sandford, T.C., and Goodell, B., (2005) “Repair of Wood Piles Using Prefabricated Fiber-Reinforced Polymer Composite Shells Journal of Performance of Constructed Facilities, 19(1), 78–87.

[17] U.S. Army Corps of Engineers (USACE). (2001). “Chapter 5: Inspection.” Unified Facilities Criteria, Naval Facilities Engineering Command and Air Force Civil Engineering Support Agency, *(UFC)— Operation and maintenance: Maintenance of waterfront facilities*, *UFC* 4-150-07, Washington, D.C.

[18] Railway track & structures. (1973). *Now: Grout-Filled Timber Piles* (Vol. 69). Bristol, Connecticut, USA: Simmons-Boardman Pub. Corp.

[19] Chellis, R. D. (1961). “Deterioration and preservation of piles.” *Pile foundations*, McGraw-Hill, New York, 339–372.

[20] Douglas, J. (1986). “Groundline repair for wood poles.” EPRI J., 29–31, April/May.

[21] Shepard, M. (1987). “Managing America’s wood pole inventory.” *EPRI J.*, 31–37, September.

[22] Hagos, M.W., (2001) “Repair of heavily decayed timber piles using Glass Fiber Reinforced Polymers, GFRP, and Cementitious grout”, Thesis Submitted to the Department of Civil and Geological Engineering; University of Manitoba; Winnipeg, Manitoba, Canada, July.

[23] Emerson, R. N. (2004). Situ Repair Technique for Decayed Timber Piles. American Society of Civil Engineers Conference Proceedings Vol. 137, No. 65.

[24] Pilemedic http://www.pilemedic.com/ [Accessed 2017]

[25] QuakeWrap http://www.quakewrap.com/ [Accessed 2017]

[26] Denso North America (Densona) http://www.densona.com/ [Accessed 2017]

[27] EN, C. (2005). 2, Eurocode 2—design of concrete structures–concrete bridges–design and detailing rules. Brussels: CEN European Committee for Standardization, 95.

[28] U.S. Department of Agriculture. (2000). “Wood Handbook, Wood as an Engineering Material, Chapter 08: Fastenings”, Washington, D.C.